SECTION I
RESEARCH IN PROGRESS

NUCLEAR REACTIONS -- EXPERIMENTAL

HIGH ENERGY GAMMA RAY PRODUCTION FROM PROTON INDUCED REACTIONS ON C, Zn, Pb AT INCIDENT ENERGIES OF 104, 145, AND 195 MeV

J. Clayton, W. Benenson, M. Cronqvist, R. Fox, D. Krofcheck, M.F. Mohar, R. Pfaff, T. Reposeur, J. Stevenson, J.S. Winfield, B. Young, C. Bloch[a] and D.E. Fields[a]

High energy photon emission from heavy ion collisions has been the subject of much study recently.[1-6] However much of the experimental effort was devoted to studying the emission from intermediate and heavy systems and little emphasis was placed on gamma ray emission from light systems. In fact there have only been two new measurements of proton-nucleus bremsstrahlung within the last 20 years. The first measurement was made by Edgington and Rose[7] in 1966. More recent measurements were made by Kwato Njock et al.[8] and by Pinston et al.[9]

Edgington and Rose studied bremsstrahlung from proton-nucleus collisions at E_p= 140 MeV. The measurement was made with a large lead glass detector. They studied bremsstrahlung from targets ranging from deuterium to lead. These measurements were thought to be correct until 1988 when Kwato Njock et al. measured proton-nucleus bremsstrahlung at an incident energy E_p= 72 MeV. They found that (compared to their value) the total cross section measured by Edgington and Rose was low by a factor 2-3. Later Pinston et al. measured proton nucleus bremsstrahlung at E_p=168 and 200 MeV and found results similar to the E_p=72 MeV data.

Both these measurement results are compared to the data of Edgington and Rose in Fig. 1. In this plot the double differential cross section is plotted as a function of the measured gamma ray energy divided by the incident proton energy. This reduced variable, E_γ/E_p, allows the comparison of the three data sets which are at different beam energies. Figure 1 demonstrates that according to this scaling law, both the data of Kwato Njock et al. and Pinston et al. are a factor of 2-3 times larger than the

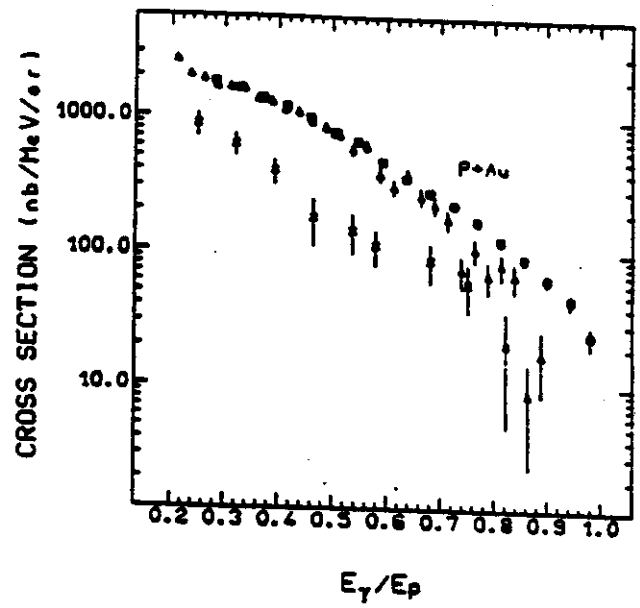

Fig. 1. Comparison of the measured spectra of Edgington and Rose to the data of Kwato Njock et al. and Pinston et al. (see text)

data of Edgington and Rose, in contrast, there is consistency in the data sets of Kwato Njock et al. and Pinston et al. even though they differ by a about a factor of 2 in incident proton energy. It should be noted that these two latter measurements were made with similar detector set ups consisting of a large NaI crystal as a calorimeter and a BaF_2 crystal to convert the incident gamma ray into an electro-positron pair. (including a BaF_2 converter gives one a detector set up with a better time resolution than the setup with the NaI crystal alone.)

We have studied proton-nucleus bremsstrahlung at incident energies of E_p=104, 145 and 195 MeV on targets of C, Zn, Pb, CD_2. The measurements were made at the Indiana University Cyclotron Facility with two 5"x9" BaF_2 crystals at angles of 45°, 60°, 90°, 120°,

and 135° in the laboratory. The BaF_2 crystals were collimated to a diameter of 8.9 cm and were placed 75 cm from the target. Between the target and the crystal a polyethylene absorber bar was placed to reduce the background from charged particles. Prompt neutrons from the target were also reduced by the polyethylene bar but the main reduction for neutrons was made by using the time-of-flight of the particles relative to the cyclotron RF. The crystals were also surrounded by a 2.54 cm thick plastic scintillator anticoincidence shield which was used to reject cosmic rays as well as charged particles from the target. The targets were all self-supporting foils which ranged in thicknesses from 25 mg/cm^2 for the Pb target to 51 mg/cm^2 for the CD_2 target.

Figure 2 shows the energy spectra for the carbon target for E_p=145 MeV at laboratory angles of θ=45°, 90° and 120°. As expected, the spectra are exponential in shape; the angular distributions are forward peaked in the laboratory. We detected photons with nearly the maximum available energy for the data at both E_p = 104 and 145 MeV. A comparison to the data

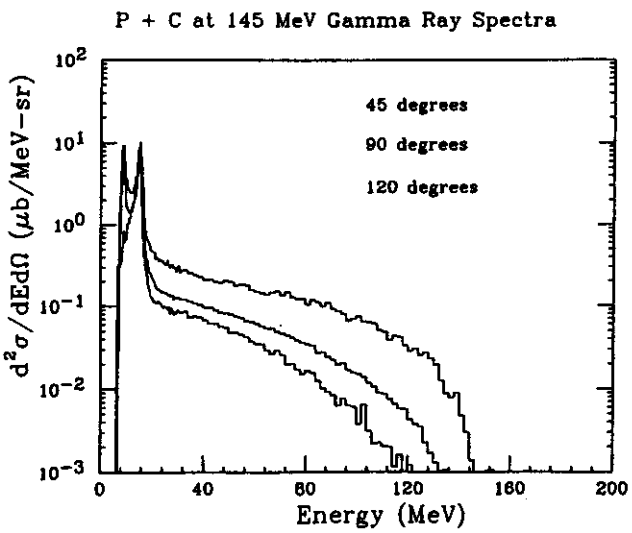

Fig. 2. The measured energy spectra for high energy gamma rays from the reaction P + C at 145 MeV.

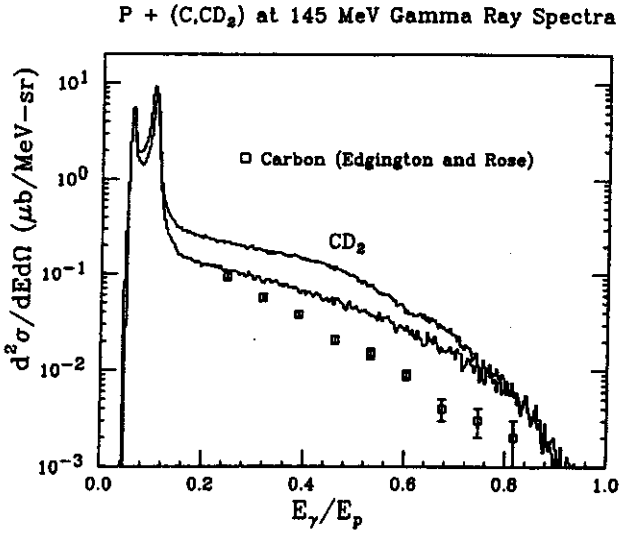

Fig. 3. Comparison of the measured spectra for high energy gamma rays from a C target and a CD_2 target at E_p=145 MeV at 90° in the laboratory. Also shown is a comparison to the data of Edgington and Rose at E_p=140 MeV.

of Edgington and Rose is shown in Fig. 3 for the C target data at E_p=145 MeV. Although the analysis is still preliminary, there is clearly a discrepancy the in the magnitude of the cross section between our data and that measured by Edgington and Rose. For gamma rays above 40 MeV in the nucleon-nucleon center-of-mass, we observe cross sections that are roughly 2-3 times greater than the cross sections reported by Edgington and Rose. In this respect, we are consistent with the measurements by Kwato Njock et al. and Pinston et al.

In the measurement of the system P + CD_2 we we will be able to extract the P + D bremsstrahlung cross section at incident proton energies of 145 and 195 MeV. This can be done by subtracting the C contribution to the spectra by normalizing the two spectra using the 15.1 MeV gamma ray transition in C. The CD_2 is compared to the C spectra in Fig. 3 at 90° in the laboratory for E_p=145 MeV. The 15.1 MeV state is easily identified in both spectra. The extracted spectra P + D is also shown in Fig. 4.

In summary we have made a series of measurements to check the data of Edgington and

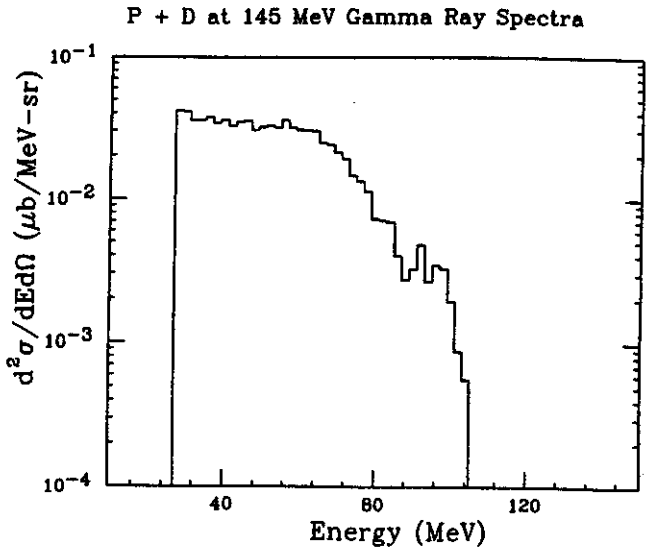

Fig. 4. The measured spectra for P + D at an incident energy of 145 MeV. The spectra was obtained by subtracting the C contribution to the spectra for the P + CD_2 target. (see text for details)

Rose. We confirm the observations of Pinston et al. and Kwato Njock et al. which indicate that the cross sections of Edgington and Rose were too small by about a factor of 2-3. Final values for the magnitude of this discrepancy will be obtained when the current analysis is complete.

---

a. Indiana University Cyclotron Facility, Bloomington Indiana.

References

1. J. Stevenson et al., Phys Rev. Lett. 57(1986)555.
2. M. Kwato Njock et al., Phys Lett. 175B(1986)125.
3. N. Alamanos et al., Phys. Rev. Lett. 173B(1986)392 .
4. E. Grosse et al., Europhys. Lett. 2(1986)9.
5. M. Kwato Njock et al., Nucl. Phys. A489(1988)368 .
6. J. Clayton et al., Phys. Rev. C40(1989)1207.
7. J.A. Edgington and B. Rose Nucl. Phys. A89(1966)523.
8. M. Kwato Njock et al., Phys. Lett. B207(1988)269.
9. J.A. Pinston et al., Phys. Lett. B218(1989)128.

FRAGMENT SPECTRA FROM $^{36}Ar+^{nat}Ag$ COLLISIONS AT 35 MEV/u

H. Hama, I Anderson, F. Deak[a], A. Galonsky, C.K. Gelbke, L. Heilbronn, A. Horvath[a], J. Kasagi[b], A. Kiss[a], D. Krofcheck, W. Lynch, T. Murakami[c], D. Sackett, Z. Seres[d], H. Schelin[e], B. Tsang and X. Yang

Emission of intermediate mass fragments (IMF) from heavy-ion collisions at intermediate energies has recieved much attention, and many possible mechanisms or processes have been discussed. In peripheral collisions, fragmentation (participant-spectator model) and/or transfer reactions dominate,[1-3] but emission from an equilibrated nucleus, which dominates at low energies, still remains at intermediate energies in spite of a low probability of complete fusion.[4] Between these extremes pre-equiliblium emission[5-7] and simultaneous multi-fragmentation[8-10] have been studied as significant mechanisms for IMF production. As these mechanisms are, however, not clearly separated from each other, many questions remain for our understanding of heavy-ion reactions.

The main purpose of our experiment was to obtain neutron-fragment coincidence data; the fragment singles reported on here are a by-product. While such inclusive data do not reveal all the details of a reaction, they are important in the overall picture of the heavy-ion collision.

The IMF energy spectra were obtained from a silver target 2.2 mg/cm^2 in thickness irradiated by a 35 MeV/u ^{36}Ar beam from the NSCL K500 cyclotron. Silicon telescopes were put at 15°, 30°, 45°, 60° and 120° with respect to the beam direction. (Neutron detectors were set at the same angles some meters behind the Si telescopes for the co-linear coincidence measurement.[11]) The δ-rays and X-rays were reduced in number by thin Au-foils which were mounted just in front of the telescopes, and most of the α-particles were eliminated by hardware rejection circuits.

The isotopes could be separated from each other by ordinary two-dimensional ΔE-E mapping. With the resulting curved particle-identification (PI) lines, however, it is quite difficult to know the background contribution because projected one-dimensional spectra involving whole energy region can never be seen. Figure 1 shows PI spectra which were linearized by applying an empirically determined formula. The weakly produced isotopes appear clearly, but the background under them is not negligible.

About 60 isotopes were extracted from linerized PI-spectra of the 15° data. The energy spectra of the most abundant isotopes of 12 elements are shown in Fig. 2. A bump on the

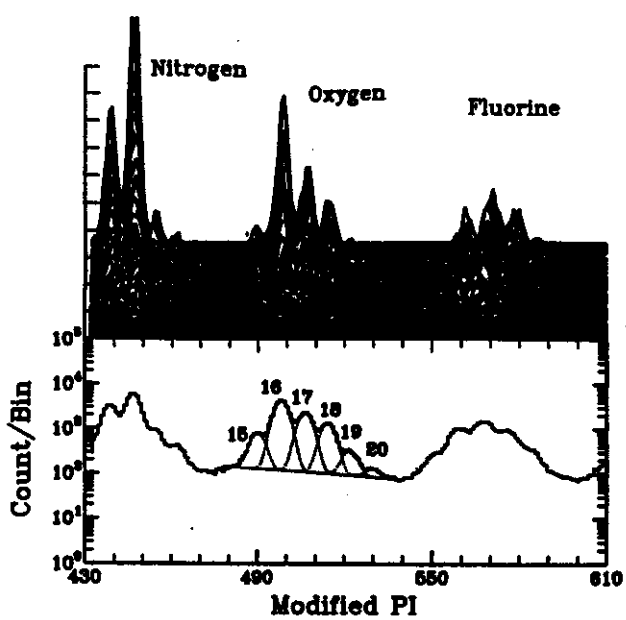

Fig. 1. Linearized PI spectrum of some 15° data. The linearization was optimized for O isotopes. The upper figure is three-dimensional; the depth coordinate has fragment energy increasing towards us. The lower figure is a projection of the upper spectrum. The intensities of six isotopes of O are obtained from a fit (dotted lines) with six Gaussians and a straight-line background.

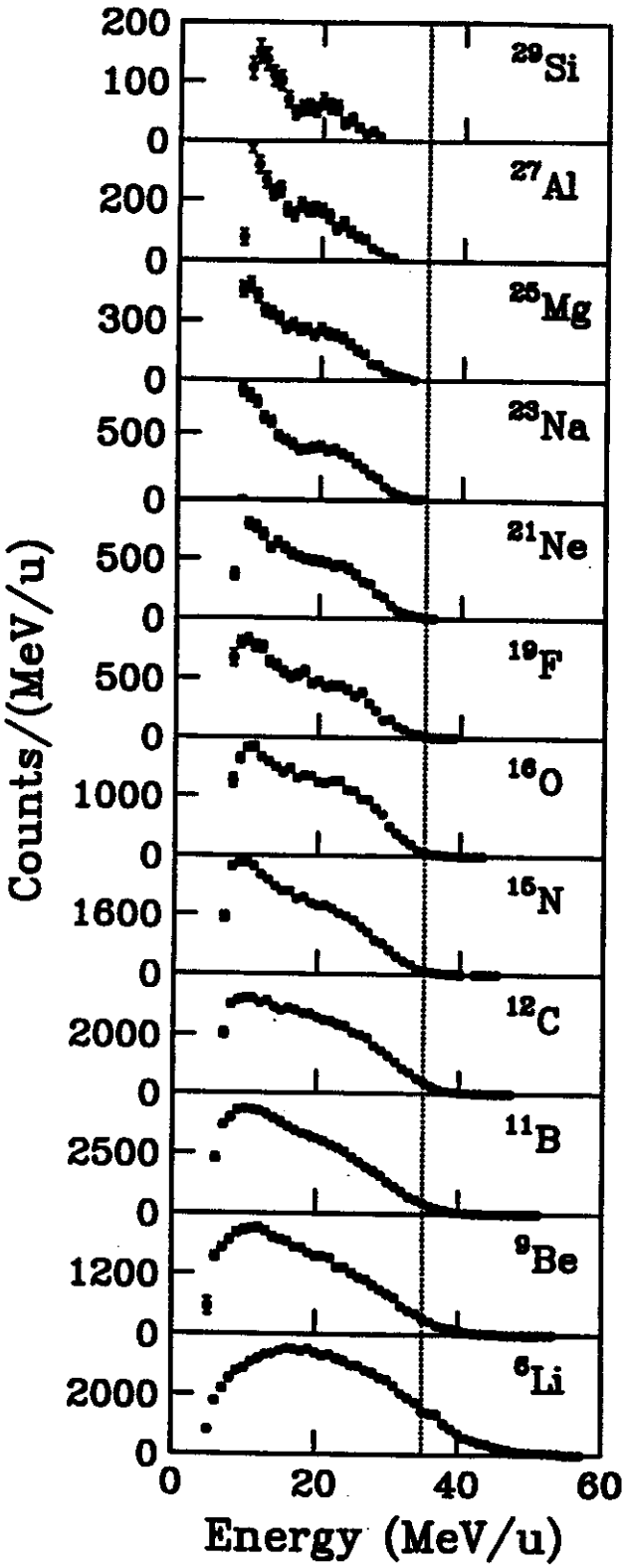

Fig. 2. The energy spectra of most abundant isotopes from Li to Si at 15°. The dotted line indicates the beam velocity.

high energy side which must be related to a quasi-elastic (QE) reaction can be seen in every spectrum. The peak position of QE component is approximately the same and at a much lower velocity than the beam velocity. At larger angles such bumps disappear and the spectra became exponentially falling in shape.

A moving source analysis was employed to reproduce energy spectra at the five angles. We assumed three sources, viz., a low-velocity target-like (TL) source, an intermediate-rapidity (IR) source, and a QE source. Maxwell-Boltzmann distributions were used for the TL and IR sources. Each of these two sources has four parameters: intensity, velocity, temperature (or slope parameter) and effective Coulomb barrier height. In accord with Goldhaber's model[1], a Gaussian shape was assumed for the momentum distribution in the rest frame of QE fragments. Here, intensity, width of momentum distrubution and mean velocity are parameters. To reduce the number of paramenters, 80% linear momentum transfer was assumed for the TL source, thus fixing its velocity parameter at 1.55 MeV/u. Assuming $E^* = (A/8)T^2$ fixed its temperature at 6.65 MeV. The fitting results for ^{6}Li and ^{16}O are shown in Fig. 3. For the ^{6}Li spectra, an overestimation can be seen on the low energy side of the 15° spectrum, while at 30° the low energy side is underestimated. Moreover, the temperature of the IR source is obviously too high. On the other hand, the fitting quality of the ^{16}O spectra are much better, although the same trend of disagreement can be seen to a lesser extent.

Figure 4 shows the fit parameters for several IMFs. The temperature of the IR source would seem to be gradually decreasing with mass. However, as typified by the fits to the ^{6}Li spectra in Fig. 3, the slopes of the spectra for the lighter IMFs indicated lower temperatures than the fits could produce. For the heavier IMFs the temperature seems independent of mass.

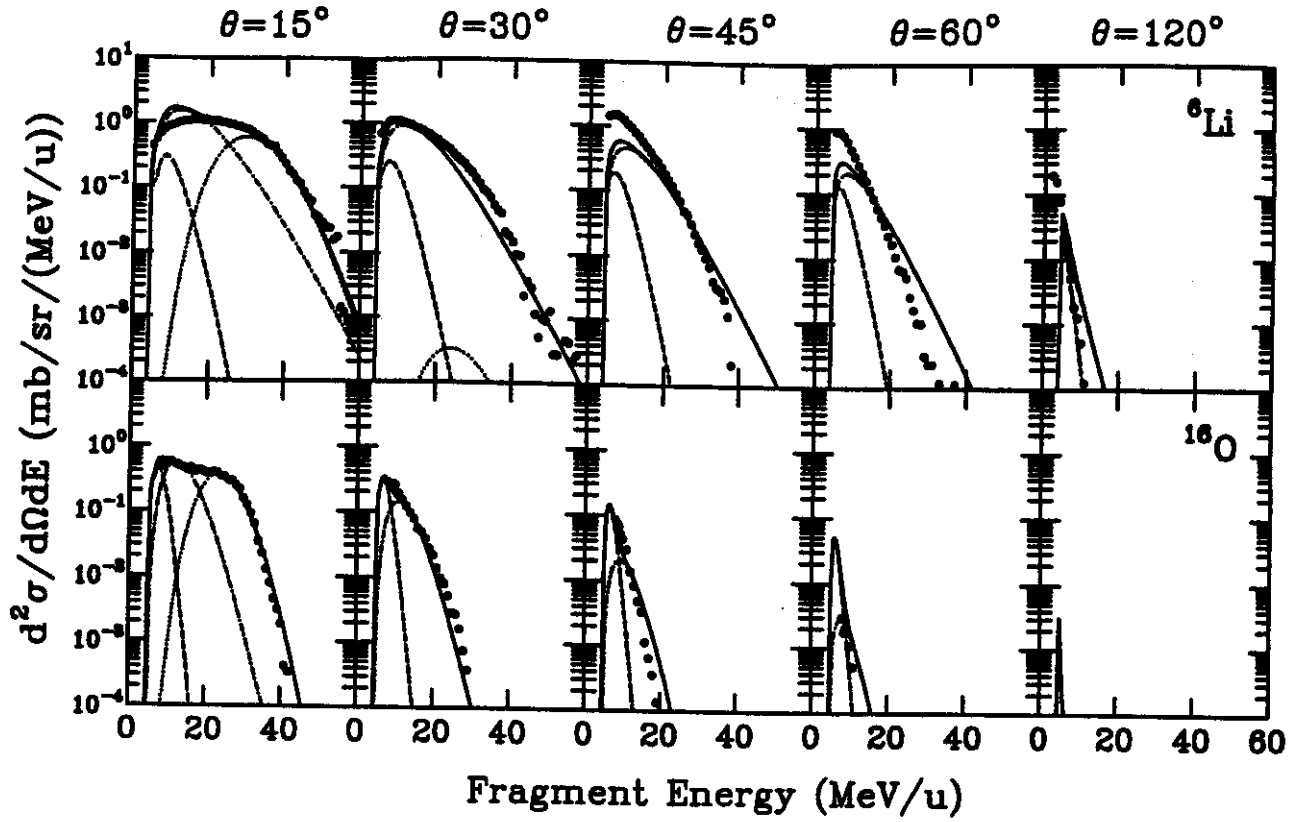

Fig. 3. The results of moving-source fits for ^{6}Li and ^{16}O fragments. The dotted lines are contributions of a QE process, the dot-dashed lines are those of an IR source, and the dashed lines are from a TL source. The solid lines are the sums of the three components.

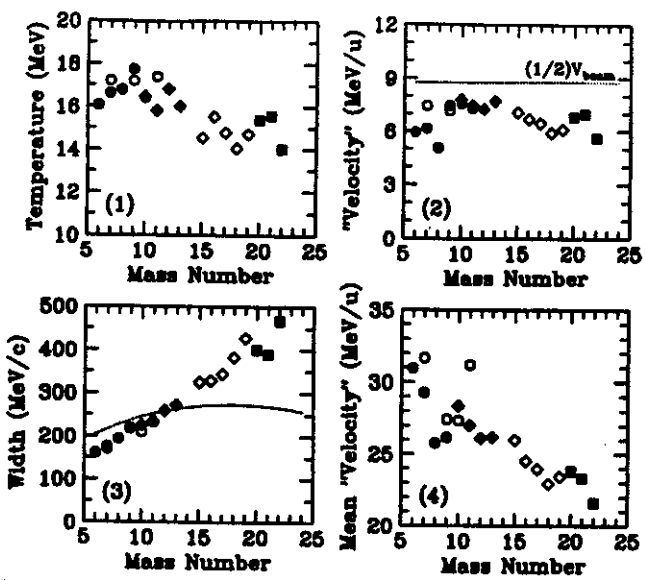

Fig. 4. The parameters of moving-source fit results for various fragments. Closed circle, open circle, closed diamond, open diamond and closed square indicate Li, Be, B, O and Ne isotopes, respectively. The upper figures sre for the IR source, the lower for the QE source. The dotted line in the width graph shows the prediction of the Goldhaber model for σ_0 = 90 MeV/c.

Velocities are also constant and close to half the velocity of the incident beam. These source properties are not inconsistent with those obtained from the experiments of others. But, because of significant disagreements mentioned above, it is hard to conclude that a moving source analysis of IMF spectra works.

The lower half of Fig. 4 shows the values of the fit parameters of the QE source. There are some difficulties here too. In Goldhaber's fragmentation model a Gaussian momentum distribution explains the shapes of fragment spectra in high energy reactions, but at intermediate energies, the distribution is known to be deformed from the Gaussian shape. In this preliminary analysis, we simply used the Goldhaber formulation to dispose of the QE contributions to the spectra.

a. Eötvös University, Budapest, Hungary
b. Tokyo Institute of Technology, Tokyo, Japan
c. Kyoto University, Kyoto, Japan
d. Central Research Laboratoty for Physics, Budapest, Hungary
e. Centro Tecnico Aerospacial, Sao Paulo, Brazil

References

1. A.S. Goldhaber, Phys. Lett. 53B(1974)306.
2. B.G. Harvey and M.J. Murphy, Phys. Lett. 130B(1983)373.
3. T. Suomijarvi, D. Beaumel, Y. Blumenfeld, N. Frascaria, J.R. Garron, J.C. Jacmart, J.C. Roynette, Ph. Chomaz, J. Barrette, B. Berthier, B. Fernandez, J. Gastebois and W. Mitting., Phys. Rev. C36(1987)2691.
4. K. Grotowski, J. Liniçki, T. Kozik, J. Lukasik, S. Micek, Z. Sosin, A. Wieloch, N. Heide, H. Jelitto, I. Kiener, H. Rebel, S. Zagromski and A.J. Cole, Phys. Lett. 223B(1989)287.
5. B. Borderie, M.F. Rivet, C. Cabot, D. Fabris, D. Gardes, H. Gauvin, F. Hanappe and J. Peter, Z. Phys. A318(1984)315.
6. D.J. Fields, W.G. Lynch, T.K. Nayak, M.b. Tsang, C.B. Chitwood, C.K. Gelbke, R. Morse, J. Wilczynski, T.C. Awes, R.L. Ferguson, F. Plasil, F.E. Obenshain and G.R. Young, Phys. Rev. C34(1986)536.
7. H.M. Xu, W.G. Lynch, C.K. Gelbke, M.B. Tsang, D.J. Fields, M.R. Maier, D.J. Morrissey, T.K. Nayak, J. Pochodzalla, D.G. Sarantites, L.G. Sobotka, M.L. Halbert and D.C. Hensely, Phys. Rev. C40(1986)186.
8. J. Randrup and S. Koonin, Nucl. Phys. A356(1981)223.
9. G. Fai and J. Randrup, Nucl. Phys. A404(1983)551.
10. D.E. Fields, K. Kwiatkowski, D. Bonser, R.W. Viola, V.E. Viola, W.G. Lynch, J. Pochodzalla, M.B. Tsang, C.K. Gelbke, D.J. Fields and S.M. Austin, Phys. Lett. 220B(1989)356.
11. F. Deak, A. Kiss, Z. Seres, G. Caskey, A. Galonsky and B. Remington, Nucl. Inst. and Meth. A258(1987)67.

IMF EMISSION IN THE ^{14}N + ^{nat}Ag, Au REACTION AT $\frac{E}{A}$ = 60-100 MeV PER NUCLEON

J.L. Wile[a], D.E. Fields[a], K. Kwiatkowski[a], K.B. Morley[a], E. Renshaw[a], V.E. Viola[a], S.J. Yennello[a], R.T. de Souza, C.K. Gelbke, W.G. Lynch, M.B. Tsang, W.G. Gong, H.M. Xu and N. Carlin

In a recently reported study[1,2] of IMF emission in the ^{14}N + ^{nat}Ag, Au system at bombarding energies of 20 to 50 MeV per nucleon, three sources of intermediate mass fragment (IMF) production were reported. The most important emission source at low bombarding energies produced IMFs with kinetic energies near the Coulomb repulsion energy and angular distributions that were relatively isotropic. The energy and angular distributions of these IMFs were well described by the model of Moretto[3]; thus, this source was identified with emission from a fully equilibrated compound nucleus. In addition to this "equilibrium" source, two other sources were observed. The first of these was associated with projectile fragmentation-like events and was analyzed using the empirical model of Kiss et al[4]. The remaining source of IMF production grew in importance as the bombarding energy was increased. The IMFs produced by this "non-equilibrium" source are more energetic than those emitted from the equilibrium source and strongly forward-focused; they constitute a significant part of the total cross section well-beyond the grazing angle. These characteristics tend to indicate that the emission takes place on a relatively short time scale. However, polarization studies[5] imply that these IMFs retain no memory of the initial beam polarization, therefore, the projectile must undergo several collisions with target nucleons before the IMF emission takes place.

In order to shed more light on the underlying mechanisms of IMF emission, as well as to investigate the possible emergence of multifragmentation as a source for IMF production, the systematics of the previous ^{14}N+^{nat}Ag, Au studies were extended to 100 MeV per nucleon. The experiment took place at the NSCL K1200 cyclotron, which delivered ^{14}N beams of 60, 80 and 100 MeV per nucleon. High-purity, self-supporting targets of ^{nat}Ag and ^{nat}Au were surrounded by seven IMF detector telescopes at 20, 50, 70, 90, 120, 140 and 160 degrees in the laboratory. The detector telescopes consisted of a CF_4 gas-ionization chamber followed by a combination of silicon strip detectors, lithium-drifted silicon detectors, and cesium-iodide crystals viewed by silicon PIN diodes. The 20 degree detector was positioned on a moveable arm and also sampled data at 35 degrees in the laboratory. Inclusive data were recorded for both targets, and the carbon contamination of the targets was found to be negligible by comparison of the silver and gold data to short runs with a carbon target.

An example of the energy spectra of boron fragments from the reaction ^{14}N + ^{nat}Ag at E_{lab} = 80 MeV per nucleon is shown for all detection angles in Fig. 1. Close examination of the figure reveals the same IMF characteristics as reported previously, i.e., high kinetic energy fragments whose cross sections drop sharply as the laboratory angle increases, and low kinetic energy fragments at backward angles whose angular distributions are rather isotropic. The data were separated into equilibrium (dotted curve), non-equilibrium (dashed curve), and projectile fragmentation (dot-dashed curve) sources by utilizing a simultaneous, three-source fitting procedure discussed elsewhere.[2] One can clearly see from the figure that the total fit (solid curve) does an excellent job of describing the energy spectra at all angles. One rather interesting result from this fit is

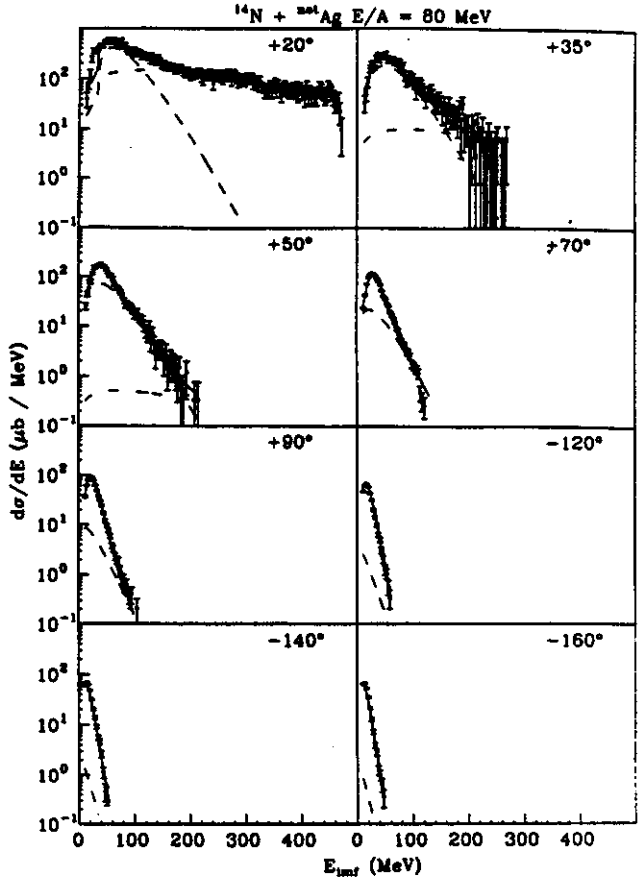

Fig. 1. Energy distributions of boron fragments from the reaction $^{14}N + ^{nat}Ag$ E = 80 MeV per nucleon. The solid curves illustrate the results of a simultaneous fit which assumes IMF emission from equilibrium (dotted), non-equilibrium (dashed), and projectile fragmentation (dot-dashed) sources. The angles indicated are in the laboratory.

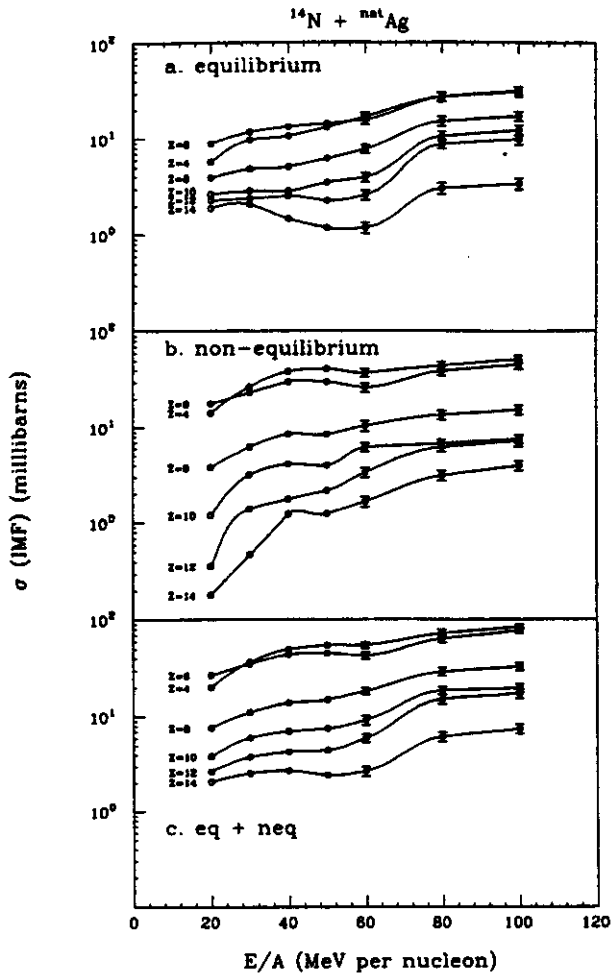

Fig. 2. IMF production cross sections for even-Z fragments from equilibrium (a), non-equilibrium (b), and both (c) sources as a function of bombarding energy. Only even-Z elements are represented. The solid curves are meant to guide the eye.

that at 100 MeV per nucleon, the temperature parameter of the equilibrium source, averaged over all elements detected, was (7.1 ± .8). If this parameter is interpreted as the actual temperature of the compound nucleus, then the data seem to indicate that nuclei can thermalize significantly more excitation energy than predicted[6], at least for this subset of the reaction cross section.

The fit discussed above allows an identification of the three IMF sources, and a determination of the IMF production cross sections from each of these sources. Figure 2 illustrates the behavior of the equilibrium (Fig. 2a) and non-equilibrium (Fig. 2b) emission cross sections for even elements as a function of bombarding energy over the entire range spanned by both this experiment and the one of Ref. 2. Although the data indicate that the evolution of the IMF production cross sections is rather smooth over the energy range studied, a few interesting points are noted. Firstly, the equilibrium emission cross sections tend to increase more rapidly for the heavier elements ($Z \geq 10$) than for the lighter ones between 60 and 80 MeV per nucleon. In the 80 to 100 MeV per nucleon range; however, the cross sections for all elements saturate. Secondly, while this

trend is quite clear for the equilibrium source, the cross sections for IMFs produced by the non-equilibrium source do not behave in a similar manner. For all elements, the non-equilibrium IMF production cross sections seem to saturate over the 60 to 100 MeV per nucleon range. The total summed cross sections (Fig. 2c) exhibit trends that essentially mirror those of the equilibrium cross sections.

The relative importance of the equilibrium and non-equilibrium sources of IMF production can be seen in Fig. 3, where the ratio of the cross section for IMFs from the non-equilibrium source to the cross section for IMFs from both sources is plotted as a function of bombarding energy per nucleon. The most striking feature of this plot is that, although the importance of the non-equilibrium mechanism as a source for IMFs increases over the low-energy range, at approximately 40-70 MeV per nucleon, depending on fragment Z, the equilibrium source starts to increase in importance. This is a reflection, of course, of the trends in Fig. 2 where, although the cross sections for non-equilibrium

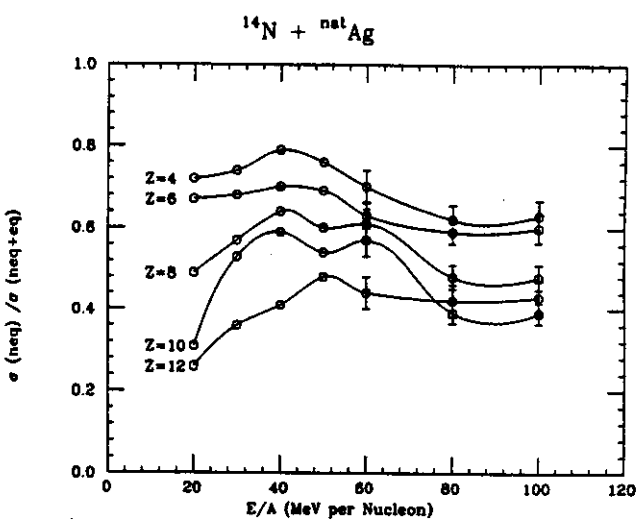

Fig. 3. The ratio of the non-equilibrium IMF production cross section to the sum of both non-equilibrium and equilibrium IMF production cross sections. The solid curves are meant to guide the eye.

IMFs increase smoothly with increasing bombarding energy, the equilibrium cross sections increase more rapidly, especially for the heavier elements.

The emission cross sections for all elements were fit as a function of atomic number with a simple power law parameterization, and the results of this fit are shown in Fig. 4. The figure shows that for the equilibrium (Fig. 4a) and summed (Fig. 4c) IMF production sources, the character of the Z distributions, as illustrated by the τ parameters, changes abruptly over to 60 to 80 MeV per nucleon range. The change in the τ parameters is actually the result of the contribution of the heavier elements as illustrated in Fig. 2. Once again, while this change is quite apparent for the two sources mentioned above, the τ parameters characterizing the Z distributions of IMFs from the non-equilibrium source do not exhibit this abrupt change in slope.

The inclusive nature of this experiment precludes any clear statement concerning both the nature of and reason for this abrupt change in emission source topology. One possible explanation would be that angular momentum is playing a more important role at higher energies, thus increasing the importance of heavy element emission from the equilibrated compound nucleus. Another possibility would be that sequential or instantaneous multifragmentation, which should be characterized by a significantly different charge distribution, may be enhancing the yield of heavy elements in the equilibrium emission source beyond $\frac{E}{A} \approx 50$ MeV. Clearly, further investigations of an exclusive nature utilizing detector systems with a large geometric efficiency must be performed to examine this phenomenon more closely.

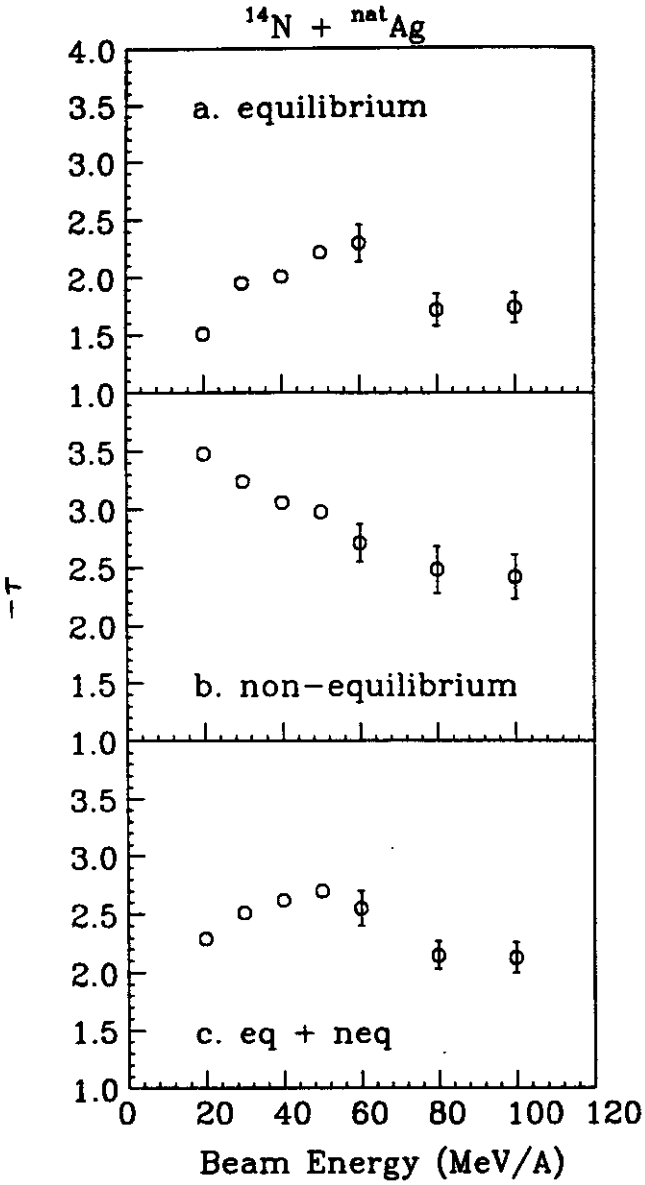

Fig. 4. The results of a fit of the IMF charge distributions using a simple Z^{τ} parameterization for the equilibrium (a), non-equilibrium (b), and the sum of the two (c) sources.

a. Indiana University Cyclotron Facility, Bloomington, IN 47405.

References

1. D.E. Fields, et al., MSU Cyclotron Laboratory Annual Report, 1987, p. 27.
2. D.E. Fields, et al., Phys. Lett. B220(1989)356.
3. L.G. Moretto, et al., Nucl. Phys. A247(1975)211.
4. A. Kiss et al., Nucl. Phys. A499(1989)131.
5. E. Renshaw, private communication.
6. D.H.E. Gross, Nucl. Phys. A437(1985)643.

PROJECTILE BREAKUP BACKGROUND IN HEAVY ION TRANSFER REACTIONS

G. Yoo, G.M. Crawley, J.S. Winfield, S. Gales[a], S. Fortier[a]

There is a substantial background in heavy ion transfer reactions which complicates the extraction of information about high lying single particle/hole states. For example, substantial backgrounds are seen at high excitation energies in single particle stripping reactions such as $^{90}Zr(^{20}Ne,^{19}Ne)$ and $^{208}Pb(^{20}Ne,^{19}Ne)$[1,2] with $E_{lab}(^{20}Ne)$ = 500, 600 and 800 MeV and $^{208}Pb(\alpha,^{3}He)$[3] with $E_{lab}(\alpha)$ = 183 MeV. The major source of the background at high excitation energies is breakup of the projectile. We are attempting to subtract this background from the spectrum by calculating the projectile breakup cross section.

There are several theoretical models for calculating the projectile breakup cross section such as the Serber Model[4], Quasifree Breakup Model (QFBM)[5], Distorted Wave Breakup Model (DWBM)[5] and the Brink-Bonaccorso Model.[6] QFBM and DWBM are principally considered as refined Serber Models. Among these we chose two models, the Serber Model and the Brink-Bonaccorso Model, and calculated the projectile breakup cross sections for the reactions of $^{208}Pb(\alpha,^{3}He)$, $^{208}Pb(^{20}Ne,^{19}Ne)$ and $^{90}Zr(^{20}Ne,^{19}Ne)$.

In calculating the cross sections with the Serber Model, we used an external wave function obtained from the Plane Wave Born Approximation[4] and the relative wave function of the constituents in the projectile. We assumed that the target is transparent to the breakup particles and the Coulomb and the spin-spin interactions between the target and the projectile are neglected. The residual nucleus and the ejectile were assumed to stay in their ground states after the breakup process. The breakup cross section is given by:

$$d^2\sigma/dE_x d\Omega_x \propto |\Psi(\vec{p})|^2 m_x (2m_x E_x)^{1/2}$$

where $\Psi(\vec{p}) = \frac{1}{h^{3/2}} \int \Psi_\alpha(r) \exp[-\frac{i}{\hbar}\vec{p}\cdot\vec{r}]d^3r$

is the Fourier transform of the relative wave function of the constituents in the projectile, m_x and E_x are the mass and energy of the ejectile after the breakup and $\vec{p} = \vec{p}_o - \vec{p}_x$ where $\vec{p}_x$, $\vec{p}_o$ are the final momentum of the ejectile and its initial momentum in the projectile. For simplicity, we chose

$$\Psi_\alpha(r) = C(\frac{\alpha}{2\pi})^{1/2} e^{-\alpha\cdot r}\frac{1}{r}(1 - e^{-\beta\cdot r})^4$$

for the relative wave function of the constituents in the projectile, where C is a normalization constant. The parameter β is determined by fitting the elastic electron scattering data and $\alpha = (2\mu\varepsilon_\alpha)^{1/2}/\hbar$ with μ and ε_α being the reduced mass and the separation energy.

The calculated cross sections are normalized to the experimental data to give the best fit and are plotted for comparison with the experimental data (Figs. 1,2). The characteristics of the breakup peaks are determined by the momentum distribution of the observed fragment in the projectile and the masses of the target and the projectile. Even though the Serber Model explained the projectile breakup background very well in light ion induced nuclear reactions[4,7,8], it does not explain the background well in the reactions $^{208}Pb(^{20}Ne,^{19}Ne)$, $^{90}Zr(^{20}Ne,^{19}Ne)$ and $^{208}Pb(\alpha,^{3}He)$. One reason is that we considered only elastic scattering, whereas a heavy target or a heavy projectile can also be excited by

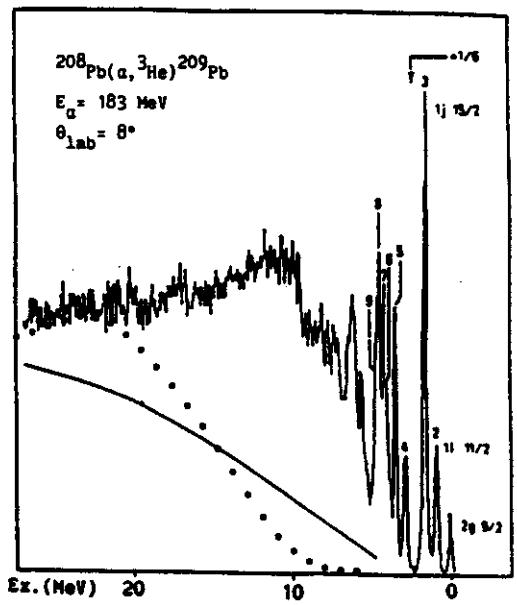

Fig. 1: Comparison of the background calculations of the α - particle breakup into ^{3}He + n with experimental data. The solid line is obtained with the Serber Model and the dotted line is obtained with the Brink-Bonaccorso Model.

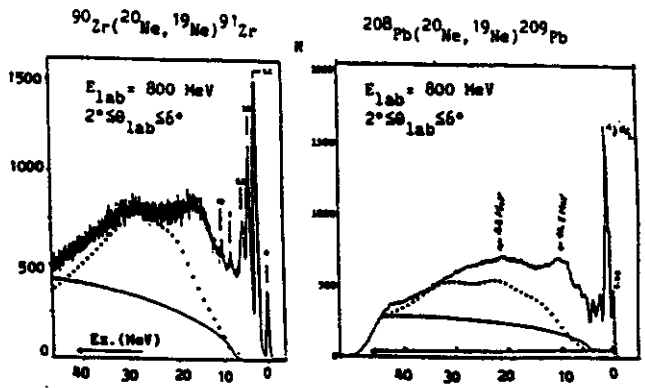

Fig. 2: a) Comparison of the background calculations of the ^{20}Ne breakup into ^{19}Ne + n at E_{lab}= 800 MeV. The solid line is obtained with the Serber Model and the dotted line is obtained with the Brink-Bonaccorso Model.

inelastic scattering. Another reason is that the only characteristics of the particles which are considered in this model are the momenta and the masses.

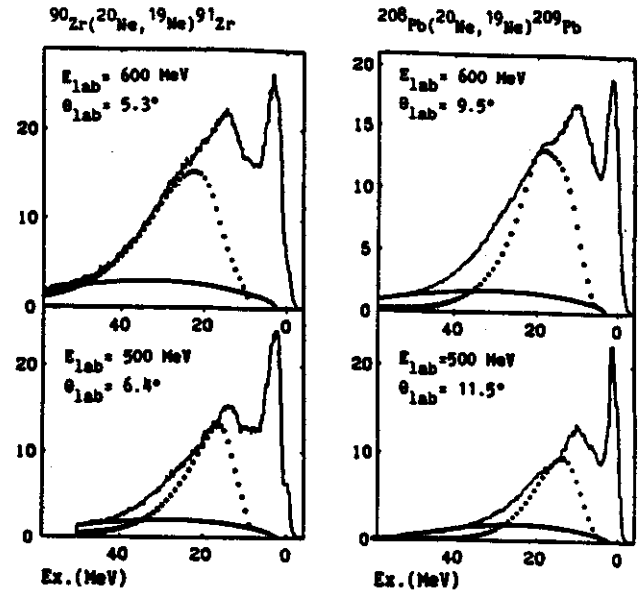

Fig. 2: b) Same comparison at E_{lab} = 500 and 600 MeV.

In calculating the projectile breakup cross sections with the Brink-Bonaccorso Model, we assumed that a nucleon makes a transition from a single particle state Ψ_i with an angular momentum L_i, J_i and energy ε_i in the first nucleus to a continuum state Ψ_f with angular momentum L_f, J_f and energy ε_f in the final nucleus. For simplicity we consider only the direct breakup process and assume that the outermost shell nucleon of the projectile is transferred to a continuum state in the target and all the particles remain in a ground state after the breakup reaction. The input values of the initial state are determined by the characteristics of the outermost valence nucleon in the projectile. The projectile breakup cross sections is given by:

$$\frac{d\sigma}{d\varepsilon} = \sum_{l_f} |1 - S_{l_f}|^2 B(l_f, l_i)$$

where $B(l_f,l_i)$ is an elementary transition probability from initial state Ψ_i to final state Ψ_f and S_{l_f} is a S_matrix element for the elastic scattering of a nucleon with energy ε by the

target. Further details of calculating the parameter $B(l_f,l_i)$ are given in Ref. 6. The S_matrix elements are obtained from the DWBA program (FRESCO) for the neutron elastic scattering reactions on targets of ^{90}Zr and ^{208}Pb by changing the bombarding energy from 2 MeV in 1 MeV steps. The optical model potential used in this analysis is

$$U(r)=-Vf(x_o) + (\frac{\hbar}{m_\pi c})^2 V_{so}\sigma L\frac{1}{r}\frac{d}{dr} f(x_{so}) -i[Wf(x_w)-4W_d\frac{d}{dx_d}]$$

where $f(x_i)=(1+e^{x_i})$, $x_i=(r-r_iA^{1/3})/a_i$, $(\frac{\hbar}{m_\pi c})^2=2.0$ (fermi)^2 and σ, L are spin and orbital angular momentum each. The same optical parameters were used throughout the whole calculations. Optical parameters and other input parameters are given in Tables 1 and 2. The calculated cross sections were also normalized to the experimental data and the maximum orbital angular momentum of a transferred neutron was determined which gave the best fit to the experimental data.

Table 1: Optical parameters for neutron elastic scattering used in this analysis.

Target	^{208}Pb	^{90}Zr
V (MeV)	69.55	45.8
r_o(fm)	1.03	1.18
a_o(fm)	0.77	0.73
W (MeV)	3.5	6.5
r_w(fm)	1.28	1.31
a_w(fm)	0.9	0.6
W_d(MeV)	2.5	3.0
R_d(fm)	1.28	1.31
a_d(fm)	0.9	0.6
V_{so}(MeV)	6.04	6.0
r_{so}(fm)	1.03	1.07
a_{so}(fm)	0.77	0.74

Table 2: Input parameters

reaction	$Energy_{lab}$ (MeV)	L_i	J_i	L_f^{max}
$^{208}Pb(\alpha,^3He)$	800	0	0.5	10
$^{208}Pb(^{20}Ne,^{19}Ne)$	500	2	2.5	7
	600	2	2.5	8
	800	2	2.5	10
$^{90}Zr(^{20}Ne,^{19}Ne)$	500	2	2.5	5
	600	2	2.5	6
	800	2	2.5	7

The calculation with the Brink-Bonaccorso Model gives somewhat better agreement to the experimental data than the Serber Model. But there are also some problems in this model. One is a divergence of the cross sections as the maximum orbital angular momentum is increased. Another is that the calculations are very sensitive to the optical parameters. Different parameters gave different results. To obtain more reliable results it will be necessary to use appropriate optical parameters for each neutron bombarding energy.

We would like to thank Prof. Brink and Prof. Bonaccorso for extensive discussions and assistance with these calculations.

---

a. Institut de Physique Nucleaire, Orsay, France

References

1. S. Fortier, S. Gales, S.M. Austin, W. Benenson, G.M. Crawley, C. Djalali, J.S. Winfield and G. Yoo, Phys. Rev. C (in press)
2. N. Frascaria et al., IPN - Orsay, Rapport Annuel, 41 (1987)
3. C.P. Massolo, F. Ajaiez, S. Gales, S. Fortier, E. Gerlic, J. Guillot, E. Hourani and J.M. Maison, Phys. Rev. C34, 1256(1986)
4. R. Serber, Phys. Rev. 72,1008(1947)
5. R.J. de Meijer and R. Kamermans, Rev. Mod. Phys., Vol.57, No.1, 147(1985)
6. A. Bonaccorso and D.M. Brink, Phys. Rev. C38, 1776(1988)
7. J.R. Wu, C.C. Chang, H.D. Holmgren and R.W. Koontz, Phys. Rev. C20, 1284(1979)
8. N. Matsuoka, A. Shimizu, K. Hosono, T. Saito, M. Kondo, H. Sakaguchi, Y. Toba, A. Goto, F. Otani, Nucl. Phys. A311, 173(1978)

$^{18}O + {}^{58}Ni$ REACTION AT 35 MeV/NUCLEON

M.C. Etchegoyen[a], A. Etchegoyen[a], A.O. Macchiavelli[b], G. Crawley, C. Djalali[c], M. Renteria[d], A. Szanto de Toledo[e] and G. Westfall

A number of studies have been made lately of reactions induced by heavy ions in the energy range between 10 and 100 MeV/nucleon.[1-4] In this region, the reaction mechanisms involved are supposed to evolve from emission from an equilibrated system at low bombarding energies, to emission from localized highly excited regions and fragmentation processes at higher incident energies.[5] The study of inclusive spectra covering this transition energy region have indicated the presence of a number of competing mechanisms. In particular, it is important to measure at very forward angles since dissipative mechanisms grow in magnitude with the detection angle.[6] Even more, at forward angles, i.e. near the grazing angle, only two mechanisms seem to be relevant, transfer and fragmentation and thus data in this angular range will hopefully yield cleaner experimental results since large low-energy dissipative tails will not be present.

In order to gain more insight into the reaction mechanisms governing this intermediate energy region, we present momentum and angular distributions of projectile-like fragments (PLF) measured in the vicinity of the grazing angle for the reaction $^{18}O + {}^{58}Ni$ at 35 MeV/nucleon, in an experiment where complete mass and charge identification have been achieved.

The experiment was carried out at the National Superconducting Cyclotron Laboratory at Michigan State University using a 35 MeV/nucleon ^{18}O beam on a self supporting ^{58}Ni target of 3.77mg/cm^2.

The emitted particles were detected using the S320 magnetic spectrograph and were measured between laboratory angles of 2 and 10 degrees, each at 8 different magnet settings in order to obtain the complete momentum spectra. Seventeen parameters associated with the PLF detection were recorded event by event on tape and unambiguous mass and charge identification was obtained by gating on various two dimensional plots of these parameters. A total of ~70 million events were obtained in three days of running time.

Ions of ^{18}O elastically scattered from a self-supporting ^{197}Au target of 2mg/cm^2 were detected between 2 and 12 degrees and at the different field settings for normalization and momentum calibration purposes. The efficiency of the detection system was also tested with the above-mentioned elastic reaction measured at 6° and for eight different magnet settings so as to cover the complete position range.

Momentum spectra for the outgoing fragments were obtained for laboratory angles θ_{lab} = 2°, 3°, 4°, 6°, 8° and 10°. The grazing angle for this reaction is θ_g = 3.8°. The typical behaviour of these fragments can be assessed from Fig. 1 for θ_{lab} = 6°, in which momentum spectra of fragment masses (A_F) ranging from 7 to 19 are plotted in increasing mass order. It is seen that those fragments with masses close to the projectile mass have narrower momentum distributions than those with smaller masses. Also, all of the spectra are peaked at momenta with velocities close to the projectile velocity, and show low-energy tails which suggest the presence of energy dissipation processes, although these tails always represent a small fraction of the measured cross section at experimental angles $\leq$ 6°. Nevertheless, this dissipation of kinetic energy is present in all fragments emitted at angles larger than the grazing angle, an effect which is obviously not

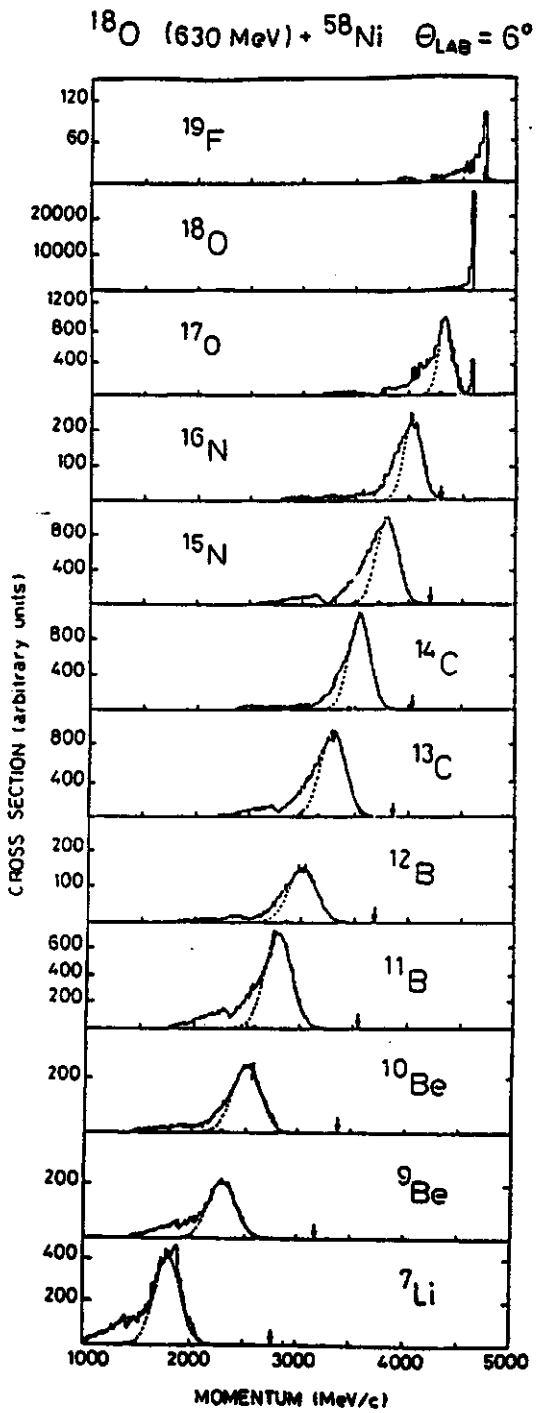

Fig. 1. Momentum spectra of outgoing fragments in the ^{18}O + ^{58}Ni reaction at $\theta_{lab} = 6°$. The dashed curves are gaussian fits to the peaks and the arrows show the fragment momentum corresponding to transfer to the ground states.

considered in the usual fragmentation models, and indicates the importance of the angle of emission in the study of reactions in this energy region.

The fragmentation model proposed by Goldhaber[7] was used to fit the experimental momentum distributions of the PLF's with gaussian distributions. The fits to the experimental momentum distributions were carried out using the high momentum part of the spectra and down to 85% of the peak maximum on the low-momentum side. These fits are displayed in Fig. 1 (dashed curves). The values of σ obtained in this fusion, were found to vary only slightly with the detection angle, as expected.

The final values, averaged over all measured angles, are plotted in Fig. 2 as a function of the mass of the ejectile where the theoretical parabolic dependence is observed to be well reproduced. The final σ values lead to σ_0 values very close to 60 MeV/c as can be seen from the solid curve depicted in Fig. 2. The weighted average of σ_0 measured for the different detected ejectiles gives a value of 60 MeV/c ± 10% as can be observed in Fig. 3. This value is low compared to the value predicted by Goldhaber's model. In this model, the high energy PLF's act as spectators, i.e., they do not interact with the target and their associated σ_0 is expected to be the width of the Fermi momentum distribution of the nucleons in the projectile. The Fermi momentum (p_F) for the nucleons in an ^{18}O nucleus is approximately[8] 230 MeV/c, a value that gives a width σ_0 of 103 MeV/c. This discrepancy could be due to the intermediate bnjkdohmey energy of the present work.

The mean momentum width measured in this work, agrees with the trend observed for the values reported between 10 and 100 MeV/nucleon of incident energy.

The experimental angular distributions were obtained from an integration over the momentum

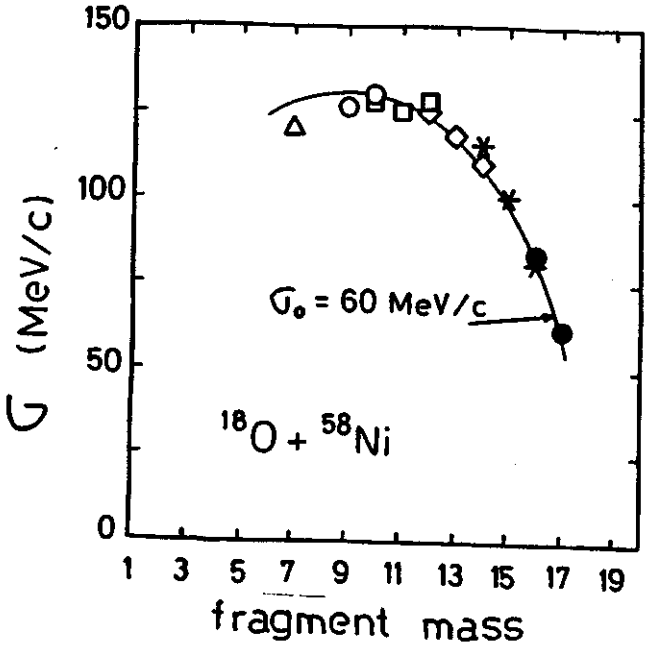

Fig. 2. Experimental and calculated momentum widths of projectile like fragments in the reaction $^{18}O + ^{58}Ni$ at 35 MeV/nucleon.

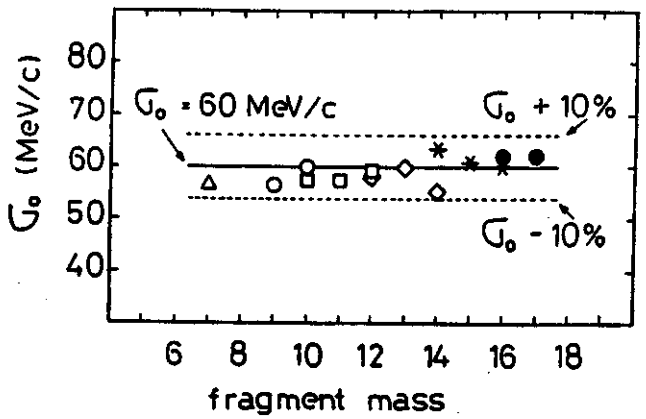

Fig. 3. Reduced momentum widths σ_o of PLF's in the reaction $^{18}O + ^{58}Ni$ at 35 MeV/nucleon.

spectra. The values of the theoretical predictions of the Goldhaber model gave distributions that decrease monotonically with angle, as observed for the actual data, but with a much steeper slope. This could be due in part to nuclear and Coulomb forces effects with are neglected in the simple fragmentation model and which are expected to be important at this intermediate bombarding energy. These forces will cause deflections of both projectile and ejectile and consequently broaden the angular distribution. This effect was considered in an approximate way in the calculations by including a shift in the deflection angle. This shift was taken as a free parameter and was optimized for the actual data. The best fits to the experimental angular distributions are obtained for PLF masses < 13 and for a shift value of ≈3° (which is similar to the grazing angle of 3.8°).

The model proposed by Cole[9] was also compared with the experimental data. In this model, angular distributions are obtained as a consequence of a "nuclear random walk" in the PLF mass. The results depend on the number of collisions between projectile and target nucleons along the classical trajectory of relative motion. Each nucleon-nucleon collision can then be described by a combination of single nucleon (neutron or proton) loss or gain and alpha-particle loss during the interaction. The model does not work at its best for our particular reaction where an ^{18}O projectile is used, since: i) in the formalism, the average number of nucleon-nucleon collisions is obtained as a convolution of projectile and target densities where parameters from electron scattering are used (charge rather than mass distribution). ii) The model supposes that the excited PLF's would emit alpha-particles and nucleons, while for the ^{18}O projectile the alpha emission would not be favoured. On the other hand, the triton emission, which may be important, is not taken into account in the formalism. iii) The model is in principle singular in the Coulomb rainbow region, and our measurements at 2° would include such contributions. Despite these disadvantages, the model gave very good agreement in shape for the angular distributions of PLF's with A > 10. The absolute cross section predicted with the random walk formalism (integrated over angles and summed over different charge values) gives good agreement with the overall trend of the experimental data.

The exponential fits which give a rather good description of the angular distributions in

the complete mass range of PLF's, are obtained using a simple expression of the form:

$$\frac{d\sigma}{d\Omega} \alpha e^{-\gamma\theta}$$

The angular distributions show a steep slope for PLF's close to the projectile mass, while for smaller masses the angular distributions look more isotropic. Similar effects, where the slope of the angular distribution increases as the fragment mass increases, are observed in a number of reactions with different projectiles and at various bombarding energies.[10,11] The explanation for such general exponential behaviour is still unclear.

Summary: New data are presented for the $^{18}O + ^{58}Ni$ reaction at 35 MeV/nucleon with complete mass and charge identification. The measurements were performed at forward angles, from 2° to 10°, which span the region in which transfer-like and fragmentation mechanisms dominate.

The bulk of the data exhibits features of high-energy fragmentation, mainly i) a parabolic mass dependence of the width of the peaks and ii) a unit ratio of ejectile to projectile velocity (v_F/v_P) for different masses and angles. Nevertheless, typical intermediate energy behaviour is also observed: i) a σ_0 value (60 MeV/c) smaller than the value = 103 MeV/c predicted by the Fermi distribution of the nucleons in the projectile. ii) low momentum contributions are always present in the momentum spectra and their relative importance increases with the detection angle, and iii) the angular distributions for PLF's with masses close to the projectile mass cannot be described by the fragmentation picture while those with A < 13 can be adequately described provided one allows a shift angle of 3°. Nevertheless, consistency with Goldhaber's predictions is observed in the sense that steeper angular distributions are obtained for fragments with smaller σ widths. The angular distributions as well as the absolute cross section can be fairly well accounted for by the nuclear random walk approach of Cole. It is apparent nevertheless that in the complete mass range the differential cross sections are best described by a simple exponential form. The smooth and striking dependence of the slope of such angular distributions on the fragment mass awaits further theoretical explanation.

We are indebted to Dr. A.J. Cole who performed the model calculations and instructed us on the model details for the reaction studied in the present work.

---

a. Consejo Nacional de Investigaciones Cientificas y Tecnicas, Argentina.
b. Lawrence Berkeley Laboratory, California 94720, USA
c. University of South Carolina
d. Universidad de La Plata, Argentina
e. Instituto de Fisica, Universidade de Sao Paulo

References

1. V. Borrel, D. Guerreau, J. Galin, B. Gatty, D. Jacquet and X. Tarrago, Z. Phys. A314(1983)191.
2. F. Rami, J.P. Coffin, G. Guillaume, B. Heusch, P. Wagner, A. Fahli and P. Fintz, Nucl Phys. A444(1985)325.
3. Y. Blumenfeld, P.H. Chomaz, N. Frascaria, J.P. Garron, J.C. Jacmart and J.C. Roynette, Nucl. Phys. A455(1986)357.
4. R. Dayras, A. Pagano, J. Barrette, B. Bertheir, D.M. Castro Rizzo, E. Chavez, O. Cisse, R. Legrain, M.C. Mermaz, E.C. Pollaco, H. Delagrange, W. Mittig, B. Heusch, R. Coniglione, G. Lanzano and A. Palmeri, Nucl. Phys. A460(1986)299.
5. D.E. Greiner, P.J. Lindstrom, H.H. Heckman, B. Cork and F.S. Bieser, Phys. Rev. Lett. 35(1975)152.
6. T. Suomijarvi, D. Beaumel, Y. Blumenfeld, N. Frascaria, J.P. Garron, J.C. Jacmart, J.C. Roynette, Ph. Chomaz, J. Barrette, B. Berthier, B. Fernandez, J. Gastebois and W. Mittig, Phys. Rev. C36(1987)2691.
7. A.S. Goldhaber, Phys. Lett. 53B(1974)306.
8. E.J. Moniz, I. Sick, R.R. Whitney, J.R. Ficenec, R.D. Kephart and W.P. Trower, Phys. Rev. Lett. 26(1971)445.
9. G. Royer, Y. Raffray, A. Oubahadou and B. Remaud, Nucl. Phys. A466(1987)139.
10. C.K. Gelbke, D.K. Scott, M. Bini, D.L. Hendrie, J.L. Laville, J. Mahoney, M.C. Mermaz and C. Olmer, Phys. Lett. 70B(1977)415.
11. G. Bizard, R. Brou, H. Doubre, A. Drouet, F. Guilbault, F. Hanappe, J.M. Harrasse, J.L. Laville, C. Lebrun, A. Oubahadou, J.P. Patry, J. Peter, G. Ployart, J.C. Steckmeyer and B. Tamain, Phys. Lett. B172(1986)301.

A TECHNIQUE FOR PROTON-DRIP LINE STUDIES VIA FUSION-EVAPORATION REACTIONS

M.F. Mohar, W. Benenson, D.J. Morrissey, R.M. Ronningen, B. Sherrill, J. Stevenson, J.S. Winfield, J. Yurkon, J. Görres[a] and K. Subotic[b]

One of our main goals in studying nuclei in the A=50 to A=100 region is to identify and study the structure of as many of these new and astrophysically important nuclei as possible. These nuclei are of interest to astrophysicists who are calculating the rp-process of nucleosynthesis and energy evolution for certain stellar environments[1-4]. Of course, any structure studies done in this region are also important in determining the single particle and collective properties of the proton-rich nuclei.

A secondary goal of our work is to be able to predict fusion/evaporation product cross sections for proton-rich nuclei. Computer codes such as ALICE[6] and CASCADE[7] are able to predict the production cross sections of stable and near-stable nuclei quite well. However, these Hauser-Feshbach based codes tend to overpredict cross sections far from stability by as much as three orders of magnitude.[8] Therefore the feasibility of a given experiment becomes difficult to judge on the basis of these uncertain predictions.

Experimental Technique

The first experiment chosen for this study was the fusion of E/A=8 MeV ^{36}Ar with a ^{40}Ca target. The beam was provided by the K500 cyclotron at the National Superconducting Cyclotron Lab, Michigan State University, and the products were identified and their momentum distributions measured in the S320 spectrograph. The reaction was chosen based on the predictions of the codes CASCADE and ALICE for producing the nuclei of astrophysical interest.

There were some demanding experimental considerations for this project. Unit Z resolution from Z=20--40 was required, and thus a detector with a wide dynamical range and an energy resolution of three to four percent was needed. Position resolution at the focal plane of better than one millimeter full width at half maximum (FWHM) was necessary in order to obtain a one-part in 600 momentum resolution. The time-of-flight (TOF) had to be measured to better than 0.8 nanoseconds FWHM to obtain a one-part in 600 velocity resolution. This combination would give the slightly better than one-part in 400 overall resolution necessary to resolve the m/q's (TOF versus position). Also, since the flight times were long compared to the cyclotron RF period, a start detector was needed at the acceptance aperture of the spectrograph and a stop detector at the focal plane. It was also important, since the 0° momentum distribution was to be measured, to separate the beam and small angle elasticly scattered ions from the reaction products before the start detector. Finally, the low energy of the evaporation products -- E/A<2 MeV -- required that the detector and detector window thicknesses be minimized in order to reduce energy-loss straggling and multiple scattering. Obviously, this requirement is related to the first three considerations -- straggling will effect the energy resolution, multiple scattering will effect the spectrograph resolution, and the need for a start detector must be weighed against the extra material it will place in the particle's path.

With these considerations in mind, the following detection scheme was designed for the S320 spectrograph. A samarium-cobalt dipole magnet was placed immediately after the target position. Since the fusion reaction products

had about half the rigidity of the beam, this magnet produced an angular separation between the evaporation products and beam velocity ions. Then, with the spectrograph set at 7° in the lab, the 0° evaporation products were transported to the spectrograph while the beam and small angle elastics in the range of 4° to 5° were collected in the Faraday cup.

The start detector was a thin-foil scintillator attached to a photomultiplier tube.[5] The foil used during the experiment was 35μg/cm^2 of Bicron BC400 plastic scintillator. The energy loss in the detector (about four or five MeV) was enough to provide an adequate start signal, and yet the detector was so thin that it did not significantly degrade the energy or momentum resolution.

The design of the focal plane detector[5] (Fig. 1) was based on the idea that the ions should be stopped in the detector volume. That way, maximum amount of energy loss (ΔE) and total energy (E) information could be used to resolve properly the Z's and to minimize the effects of ΔE straggling. This immediately implies that another position and timing detector is needed before the ΔE detector. The Breskin-type low-pressure multiwire proportional counter (LP-MWPC) was chosen as it provides both a position and a timing signal from the same detector. The position resolution

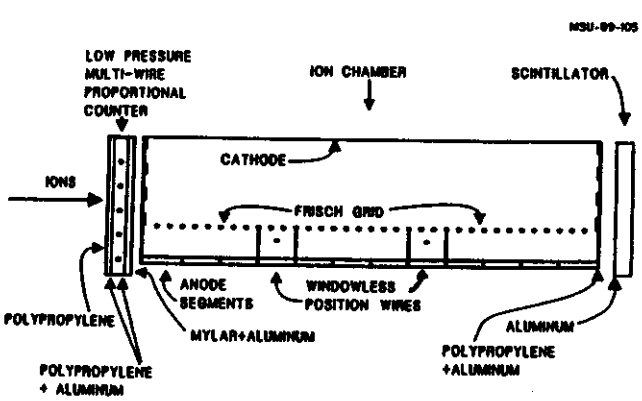

Fig. 1. S320 spectrograph focal plane detector.

was 0.7 millimeters, and the rise time of the TOF flight signal was two nanoseconds.

The evaporation products were stopped in a gas-filled ion chamber with a segmented anode. The ten one-inch segments gave a good dynamic range -- the number of segments used to create the ΔE signal could be adjusted depending on the range of the ions in the detector. A plastic scintillator in back gave the E signal for the ions that were not stopped in the ion chamber.

In addition, the angle of incidence of the products at the focal plane had to be measured in order to correct the TOF and ΔE for path-length differences. Two of the twelve anode positions in the ion chamber were occupied by resistive-wire proportional counters to give this information. The two windowless resistive wires, shown in Fig. 1, had two functions; first, they allowed the rejection of the ions that were not confined to the detector volume, and second, they provided the data necessary to calculate the angle of incidence that is needed to correct both the TOF for the angle acceptance of the spectrograph and the ΔE for the ion path in the ion chamber. The measured position resolution of the windowless wires was 0.8 millimeters FWHM.

The configuration shown in Fig. 1 was calibrated with an E/A= 2.5 MeV ^{86}Kr beam degraded to simulate the ions of interest. The calibration was used to determine the proper gas pressure and detector voltages and it provided the scale for the m/q identification (see below).

Results

Figure 2 shows a Z identification plot from the ^{36}Ar on ^{28}Si reaction. The sum of the energy loss from the first five anode strips is plotted against the sum of all ten strips, and the Z lines are clearly resolved up to Z=31 (Ga). After the Z's are resolved, the m/q

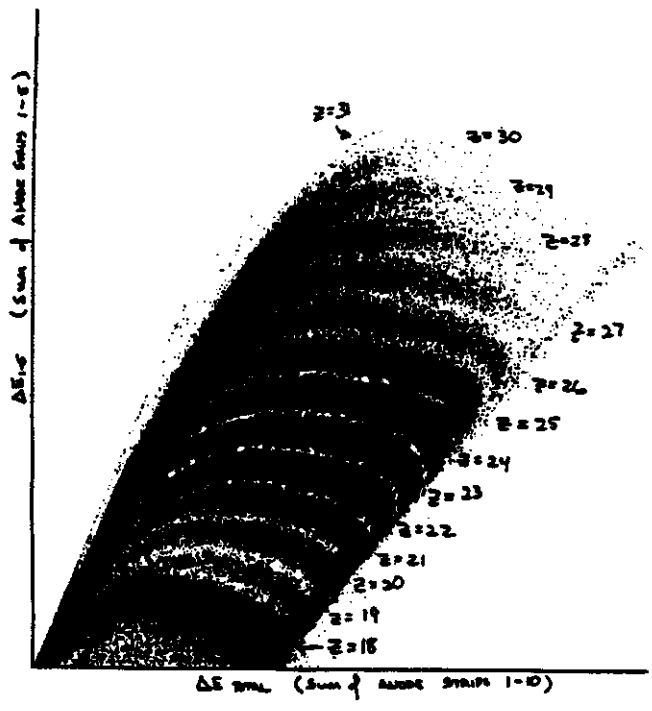

Fig. 2. Z identification plot from the segmented anode ion chamber.

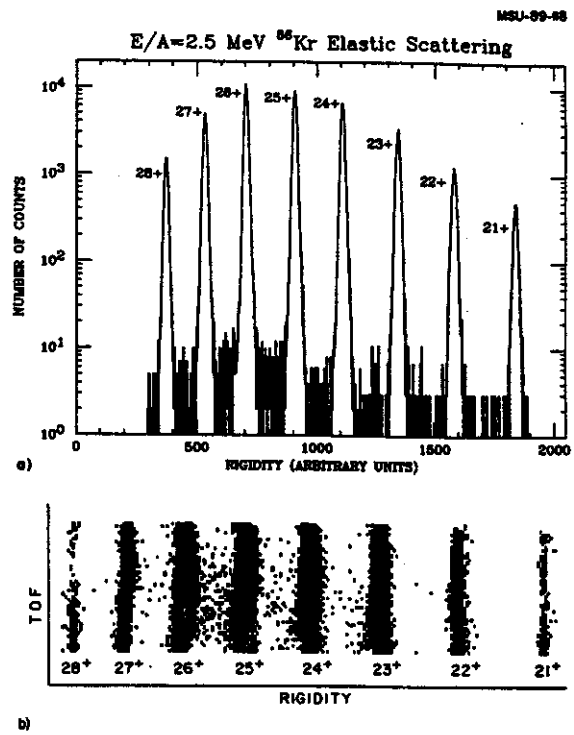

Fig. 3. a) Charge state distribution of elastically scattered E/A=2.5 MeV ^{86}Kr on an Au foil. b) An m/q plot of the same data (TOF vs. rigidity, defined as Bρ=mv/q).

spectra are constructed for each element produced in the reaction. Figure 3a shows some of the data from the E/A= 2.5 MeV ^{86}Kr calibration that illustrate the fairly broad charge state distribution for these low energy heavy ions. The two-dimensional plot of TOF versus rigidity (Fig. 3b) of the m/q's from the krypton calibration was used to identify the m/q of the evaporation products.

Figure 4 is the m/q plot (TOF vs rigidity) of the Z=29 (Cu) evaporation products from the Ar on Ca reaction. The sloped lines correspond to different m/q's of the copper isotopes. There are seven different isotopes each with as many as five different charge states. Some of the lines have double assignments. However, it is expected that when the TOF is corrected for the angle acceptance of the spectrometer the assignments should become unambiguous.

Finally, one of the m/q lines for a particular Z is selected, yielding the momentum distribution of a particular ion -- in this case $^{64}Cu^{20+}$ (Fig. 5). Again, this is shown as a function of rigidity, but because it is a single, known charge state, rigidity corresponds directly to momentum. The momentum distribution for each of the isotopes can be integrated and compared to the cross sections from the Hauser-Feshbach based codes to look for trends and deviations from the predicted values. Also, the cross sections at the peak of the momentum distributions for any exotic nuclei of interest will be known which will enable the accurate prediction of count rates in decay studies. The final task will be to do a computer simulation of the experiment to be sure that the experimental results are reproducible when all of the cross sections, detector thicknesses, and spectrometer acceptances are included.

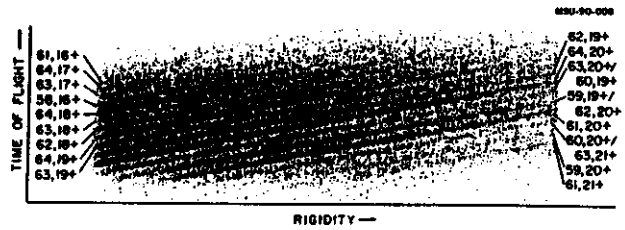

Fig. 4. An m/q plot of copper ions (Z=29).

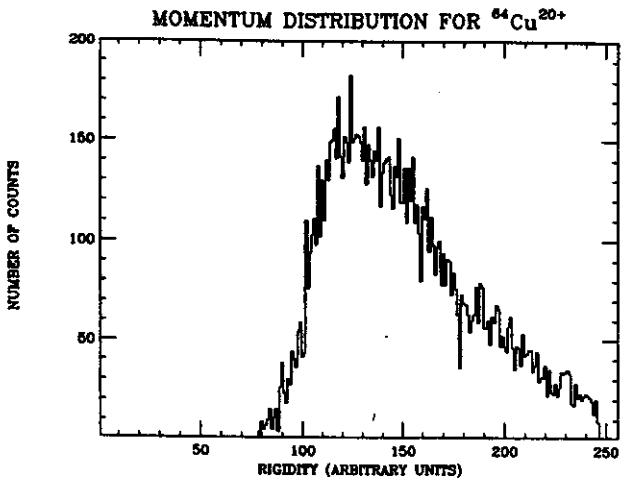

Fig. 5. Rigidity plot of $^{64}Cu^{20+}$. Since only one charge state of ^{64}Cu is plotted, the rigidity distribution corresponds directly to a momentum distribution.

a. Department of Physics, University of Notre Dame, Notre Dame, IN 46556
b. Physics Dept.-010, Boris Kidrich Institute, POB 533, 11001 Beograd, Yugoslavia

References

1. R.K. Wallace and S.E. Woosley, Astrophys. Journ. Suppl. 45(1981)389.
2. S.E. Woosley, Procedings of the Accelerated Radioactive Beams Workshop, eds. L. Buchmann, J.M. D'Auria, Parksville, Canada, p.4, 1985, and references therein.
3. R.K. Wallace and S.E. Woosley, High Energy Transients in Astrophysics, ed. S.E. Woosley, AIP Conf. Proc. No. 115, New York, p. 319.
3. W.H.G. Lewin and P.C. Joss, Accretion Driven Stellar X-Ray Sources, eds. W.Lewin, E. van den Heuvel, Cambridge Univ. Press, Cambridge, p. 41.
4. M.F. Mohar et al., NSCL/MSU Annual Report, 1988.
5. F. Plasil, Phys. Rev. C 17(1978)823.
6. F. Puhlhofer, Nucl. Phys. A280(1977)267.
8. Comparison of calculations from CASCADE and ALICE to results of C.J. Lister et al. in Nuclei Far From Stability, ed. Ian S. Towner, AIP Conf. Proc. No. 164, Rosseau Lake, Ontario, Canada, 1987, page 354.
9. Norbeck, Dubbs, and Sobotka, Nucl. Instr. and Meth. A262(1987)546.
7. A. Breskin, Nucl. Instr. Meth. 196(1982)11.

SPIN-POLARIZED RADIOACTIVE ISOTOPE BEAMS FROM INTERMEDIATE ENERGY HEAVY-ION COLLISIONS

K. Asahi[a], M. Ishihara[a], N. Inabe[a], T. Ichihara[a], T. Kubo[a], M. Adachi[b] H. Takanashi[b], M. Kouguchi[b], M. Fukuda[b], D. Mikolas, D.J. Morrissey, D. Beaumel[c], T. Shimoda[d], H. Miyatake[d] and N. Takahashi[d]

We have studied the spin polarization of projectile-like fragments emitted in an intermediate-energy heavy ion reaction. Specifically, we have measured the spin polarization of ^{12}B fragments produced in the ^{14}N + ^{197}Au reaction at E/A = 40 MeV/nucleon, as a function of ^{12}B momentum. The polarization was determined by the observation of a β-ray asymmetry in the decays of $^{12}B_{g.s.}$ ($I^{\pi} = 1^{+}$, $T_{1/2} = 20.20$ ms, $Q_{\beta} = 13.369$ MeV) to $^{12}C_{g.s.}$ ($I^{\pi} = 0^{+}$).

A 97-mg/cm^2 thick ^{197}Au target was bombarded with ^{14}N ions from RIKEN Ring Cyclotron in Tokyo, Japan. The effective incident energy, corrected for the energy loss at one-half the target thickness, was 39.4 MeV/nucleon. The relatively thin target was chosen so that the initial momentum distribution of the emerging fragment were not significantly distorted by the energy loss. Fragments emitted from the target at an angle of $\theta_L = 5°$ were momentum-analyzed with a dipole magnet and focused by means of a quadrupole doublet. The ^{12}B products were stopped in a Pt foil (200-μm thick) located at the focus after passing through an energy degrader. A collimator with a 7 mm diameter hole was placed 7 cm upstream of the focus to select fragment momenta with $\Delta p_f/p_f = \pm 0.5\%$. This selection also served to reduce contributions from background β-emitters with different A/Z values. Thus only ^{8}Li and ^{13}B activities made noticeable background contributions.

A static magnetic field, $B_0 = 58.3$ mT, in the direction normal to the reaction plane was applied to the stopper in order to preserve the polarization of implanted ^{12}B fragments. The spin lattice relaxatioh time for ^{12}B in Pt at room temperature is much longer than the lifetime of the ^{12}B nucleus in such a field. The β rays from the ^{12}B decays emitted in the direction perpendicular to the reaction plane were detected with plastic scintillation counter telescopes located above and below the stopper. The angular distribution of β rays from nuclei with a polarization P is given by $W(\theta) = 1 - (v/c)AP\cos\theta$, where θ is the angle of β ray emission relative to the polarization axis, A is the asymmetry parameter, and v/c the velocity of β particles. In our convention, θ=0 corresponds to the detection of β^- particles along the reaction normal $\hat{7}=\vec{p_i} \times \vec{p_f}/|\vec{p_i} \times \vec{p_f}|$ where $\vec{p_i}$ and $\vec{p_f}$ are the momentum gate beam and detector ^{12}B fragment, respectively. Noting that v/c = 1 and inserting A = -1 for the $^{12}B_{g.s.} \rightarrow {}^{12}C_{g.s.}$ decay, the ratio of the up/down β-ray counting rates can be written as $U/D = (1 - P)/(1 + P)$. This relationship could be inverted to obtain the polarization P given the ration u/p.

In measurements of β decay asymmetry it is very important to remove systematic biases of the detectors. This was accomplished by calculating the polarization from a double ratio of the Up/Down counting rates. The cyclotron beam was pulsed on for 30 ms and off for 30 ms loading the Pt stopper with boron nuclei. Counting of the β rays began 3 ms after the end of the beam-On cycle giving the first measurement of the Up/Down ratio. In addition, the spin polarization was artificially reversed at the end of every-other beam-On period by taking the spins through an adiabatic fast passage of their nuclear magnetic resonance. (This is accomplished by exciting a small rf coil placed around the stopper during the first 3 ms of the beam-Off period producing an oscillating magnetic field, B_1, perpendicular to

B_0. The frequency of B_1 is swept across the Larmor frequency, e.g., ν = 444 kHz for ^{12}B (g.s.), which flips the polarization axis.) In the subsequent beam-Off cycle the rf field is swept over a different but similar frequency range leaving the spin polarization undisturbed. Experimental volumes for the polarization were thus calculated from the double ratio: R = {[Up/Down] off-resonance / [Up/Down] on-resonance} with the expression: $P = (1 - \sqrt{R}) / (1 + \sqrt{R})$. The values of P were corrected for reduction due to any background activities (^{8}Li and ^{13}B were the only contaminants) and for ^{12}B which survives from the previous beam-Off cycle.

The experimental results are presented in Fig. 1. The momentum distribution of the ^{12}B fragments, shown in the lower part, exhibits a single broad peak with a maximum located close to the momentum corresponding to the incident beam velocity. The shape is nearly Gaussian, although it is slightly asymmetric, extending more towards lower momenta. The width σ deduced from the higher momentum side is consistent with the Goldhaber formula ($\sigma = \sigma_0[A_F(A_p-A_F)/(A_p-1)]^{1/2}$ where A_F and A_p are the projectile and the fragment masses) if we take a value of σ_0 = 74 MeV/c, slightly smaller than those obtained at relativistic energies. These features are typical of projectile fragmentation processes at intermediate energies.

The measured spin polarization of ^{12}B fragments is shown in the upper part of Fig. 1 as a function of ^{12}B momentum. The sign of P is defined as such that P > 0 when the spin is parallel to the vector $\vec{p}_i \times \vec{p}_f$. A remarkable feature of our results is the change in sign of the polarization as a function of momentum. The sign change occurs near the peak of the yield. Also the size of the polarization is surprisingly large, reaching 20% at the maximum. There is a small difference in magnitude between the high and low momentum sides, which may be related to the asymmetry in the shape of momentum distribution.

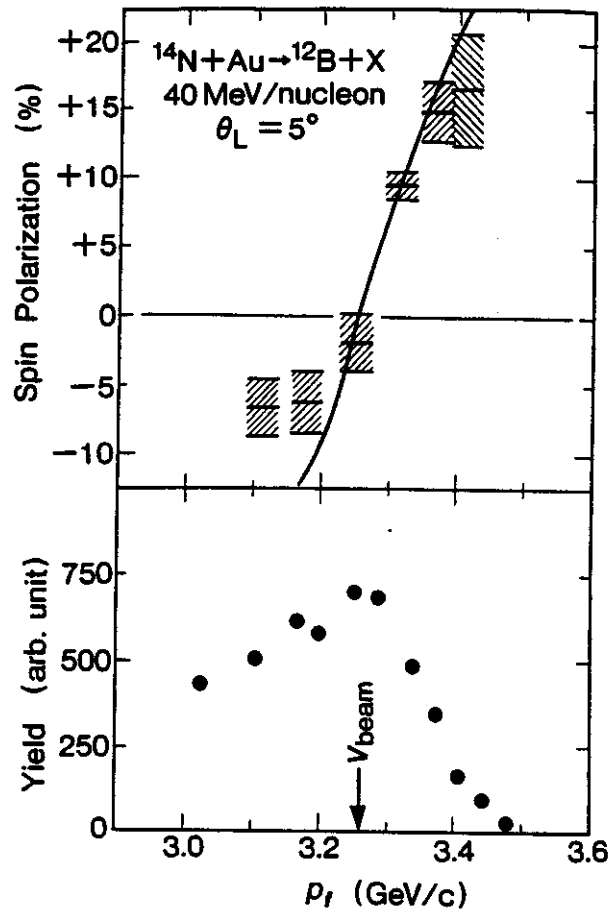

Fig. 1. Spin polarization (upper part) and yield (lower part) for ^{12}B fragments are shown as functions of the outgoing momentum. The solid curve represents the result of a calculation based on a simple picture of projectile fragmentation.

The experimental results appear to shed new light on the inherent nature of the projectile fragmentation process. Let us consider a peripheral collision of a projectile nucleus with a target in which the nucleons in the overlapping volume are removed from the projectile and the resulting nucleus is observed as an outgoing fragment. The essential assumptions of this picture are that the fragment part remains as a spectator and emerges with a positive scattering angle. Corresponding to a predominantly repulsive momentum transfer between projectile and target caused by their mutual Coulomb interactions. In this framework there exists an interesting correlation between

the outgoing momentum p_f and the internal angular momentum J of the fragment. One can easily see this correlation by noting the expressions, $\vec{p}_f = m\vec{v}_0 - \vec{k}_r$ and $J = -\vec{R} \times \vec{k}_r$, where m and $\vec{v}_0$ are the fragment mass and the projectile velocity, respectively, and $\vec{R}$ is the position vector pointing from the fragment to the removed portion. These expressions are obtained based on the conservation laws of linear and angular momenta and both are given in terms of the momentum in the projectile-rest frame, $\vec{k}_r$, which is carried before the collision by the removed portion. The latter expression arises since J of the resultant fragment plus the angular momentum carried by the removed portion ($\vec{R} \times \vec{k}_r$) should make up the projectile spin. (We assume zero spin of the projectile and ignore the intrinsic spins of removed nucleons for simplicity.)

Thus, processes associated with $\vec{k}_r$ parallel to the beam direction ($k_r{}^z > 0$) should correspond to events of lower p_f and favor negative polarization ($P < 0$) as opposed to those with $k_r{}^z < 0$ lead to events of high p_f and $P > 0$. The signs of the polarizations predicted by this simple model would be reversed, however, if the ^{12}B fragment emerged instead at negative scattering angles characteristic of attractive momentum transfers. The observed behavior of the sense of P nicely agrees with this simple argument and the assumption of positive scattering angles. The magnitude of polarization is expected to be the same for the low- and high-momentum sides, while a slight reduction is observed for the former. This, as well as the distortion in the yield spectrum, indicates that more complicated reaction processes and possibly, negative scattering angles may also contribute to the low-momentum region.

In conclusion, we have measured the spin polarization of the projectile-like fragment ^{12}B in $^{14}N + ^{197}Au$ reactions at an intermediate energy. The result shows sizable polarizations ($|P| = 5$-20%) over the whole range of the fragment momentum distribution except for the momentum corresponding to the beam velocity. The consistency between the experiment and the general kinematical arguments strongly suggests that this polarization phenomenon may be universal over the intermediate energy projectile fragmentation reactions. This feature combined with the observed large polarization provides promising prospects for production of polarized beams of radioisotopes.

---

a. Insititute of Physical and Chemical Research (RIKEN), Wago-shi, Saitama 351, Japan.
b. Department of Applied Physics, Tokyo Institute of Technology, Oh-okayama, Tokyo 152, Japan
c. Institute de Physique Nucleaire, B.P. 1, 91406 Orsay, France.
d. College of Generald Education, Osaka University, Toyonaka, Osaka 560, Japan.

FRAGMENT PRODUCTION MEASUREMENT USING PLASTIC TRACK DETECTORS

K. Subotic[a], D. Novkovic[a], M. Stojanovic[a], B. Stepancic[a], B. Grabez[a] and R.M. Ronningen

In intermediate energy heavy ion collisions light fragments ($3 \leq Z \leq 26$) having velocities lower than the beam velocity are thought to be products of target fragmentation. In the interaction of 84 MeV/nucleon ^{12}C with ^{208}Pb these fragments were determined to come primarily from a binary breakup of the target.[1]

Understanding the mechanism for low energy light fragment production requires exclusive measurements and systematical studies. We are testing the suitablity of plastic track detectors at the NSCL to make such measurements.

Targets of isotopically enriched ^{7}Li, ^{27}Al, and ^{208}Pb , whose thicknesses were approximately 0.4 μm, were sandwiched between two sheets of CR-39 track detecting plastic. This enabled reaction products to be detected and correlated in nearly a 4π geometry. A third sheet of CR-39 behind the sandwich acted as a beam monitor. A beam of 85 MeV/nucleon $^{20}Ne^{7+}$ was defocussed to uniformly irradiate each target over a 4 cm^2 area. Each target was irradiated for 5 seconds at an intensity of 10 epA. The CR-39 was then analyzed at the Boris Kidrich Institute using the techniques described in Ref. 1.

Figure 1 shows the frequency distribution of light fragment charges for the Al target. We have learned from this test that plastic track detectors can be employed for such measurements at the NSCL but a somewhat higher particle dose is needed for better statistics. Another measurement will be made using a 100 MeV/nucleon beam.

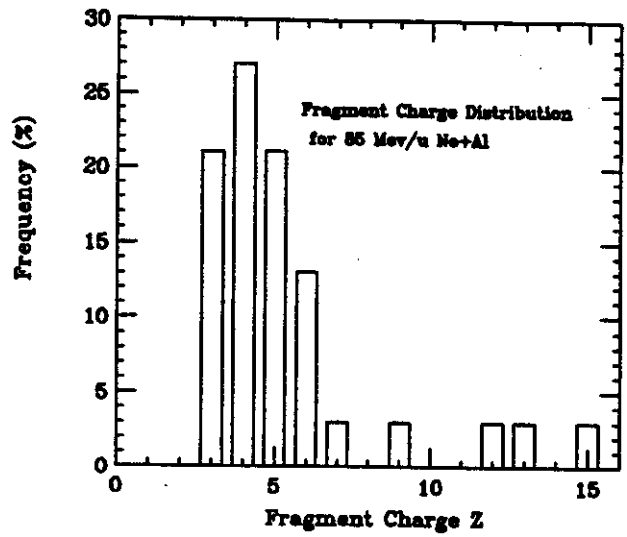

Fig. 1. Frequency distribution of low energy, light fragment charges in the reaction of 85 MeV/nucleon ^{20}Ne with ^{27}Al.

a. Boris Kidrich Institute, Beograd, Yugoslovia

References

1. B. Grabez, R. Beckmann, P. Vater and R. Brandt, Phys. Rev. C. 34(1986)170.

PRODUCTION CROSS-SECTIONS OF P^+, D, T, ^3He, and α FOR La + La 800 MeV/N NUCLEAR COLLISION

J. Bistirlich[a], H. Bossy[a], T. Case[a], A. Chacon[a], K.M. Crowe[a], Y. Dardenne, W. McHarris, J.O. Rasmussen[a] and M. Stoyer[a]

The question of the degree of nuclear flow in high-energy nucleus-nucleus collisions remains an on-going one. Many different models have been formulated, from simple intramolecular-cascade models to hydrodynamical models to models that include Δ-resonance effects. Measuring the cross-sections for the production of light fragments from the collisions of very heavy relativistic nuclei seems to be important for sensitive tests of such models.

The only published experimental results are those of Hayashi et al.[1] for 0.8-GeV/A ^{139}La + ^{139}La collisions. A recent comparison of the data with various theories shows significant disagreement, as shown in Fig. 1. Here the comparison is with three Cascade models [Frankel-Yariv (FY), original Cugnon (CG1), and latest Cugnon (CG2)] and four Cascade-Mean-Field models [Vlasov-Uehling-Uhlenbeck (VUU), Quantum Molecular Dynamics (QMD), Boltzmann-Uehling-Uhlenbeck (BUU), and Relativistic VUU (RVU)]. The comparisons were made for 20°, 40°, and 60° (lab).

The points to notice are: 1) The general shape of the curves is reproduced by most models. 2) There is significant discrepancy at 20°. 3) The models, especially the transport models, agree very well with one another. This last point is surprising, considering that there are significant differences between the various theoretical approaches.

Since the various models agree so well but not with the data, we decided to reproduce the data, modifying the JANUS spectrometer at the LBL Bevelac, making use of reverse kinematics.[3] Figure 2 shows an upper view of JANUS: This set-up was placed on a turntable so as to reproduce

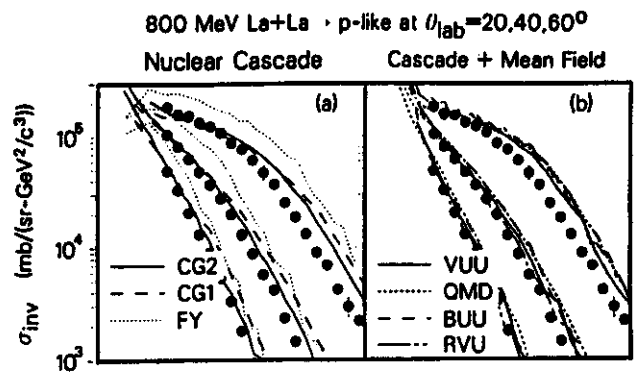

Fig. 1. Comparison of nuclear transport calculation to data (ref 2). (a) Comparison of Cugnon cascade model versions CG1 and CG2 with the Fraenkel-Yariv cascade model (FY). (b) Comparison of momentum independent VUU and QMD models to momentum dependent BUU and RVU models.

the angles both of agreement and disagreement. A field of 7 KG was applied to the magnet, and the multi-wire proportional counters (MWPC) were used to determine the rigidity of the outgoing particles. Plastic scintillators were used as start triggers (S1 and S2) for time-of-flight measurements and also as stop triggers (AB). The A array was divided into eight counters, the B array into ten, the overlap of A_i with B_j segmented the active area of MWPC 4.

In this experiment, particle identification is achieved via rigidity plus TOF measurements.

The experiment was carried out in January 1990, and data are now being analyzed. Currently, the acceptance of the spectrometer is being calculated and energy-loss and scattering effects in the various media are being determined. Figure 3 shows a current set of trajectories calculated via Monte Carlo simulations.[4]

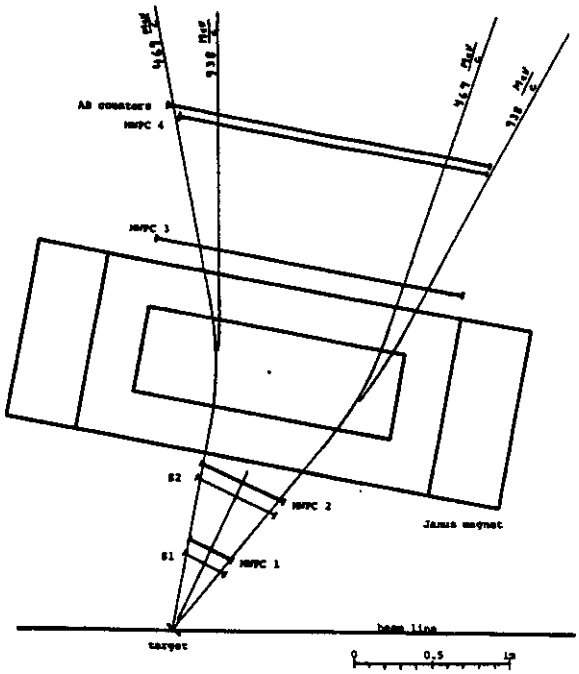

Fig. 2. JANUS spectrometer.

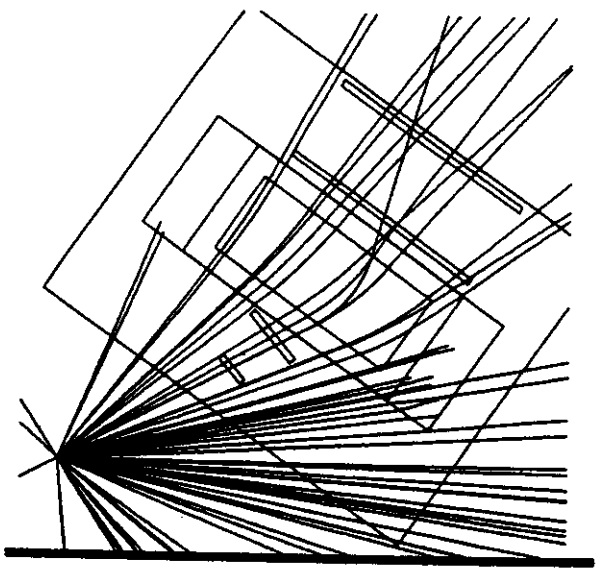

Fig. 3. Calculated trajectories.

a. Nuclear Science Division Lawrence Berkeley Laboratory, University of California, Berkeley, California 94720.

References

1. S. Hayashi, Y. Miake, T. Nagar, S. Nagamiya, H. Hamagaki, O. Hashimoto, Y. Shida, I. Tanikata, K. Kimura, O. Yamakawa, T. Kobayashi, and X. X. Bai, Phys. Rev. C 38(1988)1229.
2. J. Aichelin, J. Cugnon, Z. Fraenkel, K. Frankel, C. Gale, M. Gyulassy, D. Keane, C. M. Ko, J. Randrup, A. Rosenhauer, H. Stoker, G. Welke, and J. Q. Wu, Phys. Rev. Lett. 62(1989)1461.
3. J. Bisterlich, H. Bossy, T. Case, A. Chacon, K. Crowe, M. Justice, J. O. Rasmussen, and M. Stoyer, LBL Bevelac Proposal (1989).
4. G. Fai, J. Randrup, LBL report LBL-21573 (Aug, 1986).

AZIMUTHAL DISTRIBUTIONS OF FISSION FRAGMENTS AND α-PARTICLES EMITTED IN THE REACTIONS $^{36}Ar+^{238}U$ AT E/A=20 AND 35 MeV AND $^{14}N+^{238}U$ AT E/A=50 MeV

M.B. Tsang, Y.D. Kim, N. Carlin, Z. Chen, C.K. Gelbke, W.G. Gong, W.G. Lynch, T. Murakami, T. Nayak, R.M. Ronningen, H.M. Xu, F. Zhu
L.G. Sobotka[a], D.W. Stracener[a], D.G. Sarantites[a], Z. Majka[a] and V. Abenante[a]

In order to explore the distribution of particles in and out of the reaction plane and to explore techniques for reaction plane determination, we have investigated correlations between coincident fission fragments and α-particles emitted in the reactions $^{36}Ar+^{238}U$ at E/A=20 and 35 MeV and $^{14}N+^{238}U$ at E/A=50 MeV. The experiment was performed with beams from the K500 cyclotron of Michigan State University. A $^{238}UF_4$ target of 400 μg/cm^2 areal density was used. Charged particles were detected with 96 plastic CsI(Tl) phoswich detectors of the "Dwarf-Ball-Wall" array developed at Washington University[1], which provided an angular coverage of about 85% of 4π. Two coincident fission fragments were detected with two X-Y-position sensitive multiwire detectors[2] covering angular ranges of θ_1=36°-116° for ϕ_1=0±10° and θ_2=39°-89° for ϕ_2=180±30°. All data were filtered with appropriate gates on the fission fragment folding angles in order to reduce contributions from peripheral collisions. Unless otherwise stated, all angles and energies are given with respect to the laboratory frame of reference. Polar angles with respect to the beam axis are denoted as θ and azimuthal angles are denoted as φ.

The left hand panels of Fig. 1 show the azimuthal distribution, $Y_\alpha^{ff}(\phi_\alpha)$, of α-particles emitted at θ_α=70° and with energy E_α=46-70 MeV in coincidence with two fission fragments; the fission plane is defined as ϕ_α=0° or 180°. (Azimuthal correlations presented in this report are normalized to an average value of unity. Open squares, solid points, and open circles show data for the reactions $^{36}Ar+^{238}U$ at E/A=20 and 35 MeV and $^{14}N+^{238}U$ at E/A=50 MeV, respectively.) Consistent with previous observations[3], these particles are preferentially emitted in the fission plane. For the decay of residues with large angular momenta, the fission plane is closely correlated with the entrance channel reaction plane. In order to extract the azimuthal anisotropies, $R_\alpha^{ff} = Y_\alpha^{ff}(\phi_\alpha=0°)/Y_\alpha^{ff}(\phi_\alpha=90°)$, we have fitted the azimuthal distribution with a simple functional form: $Y_\alpha^{ff}(\phi_\alpha) \propto \exp(-\kappa \sin^2\phi_\alpha)$, where κ was treated as an adjustable parameter. Examples of

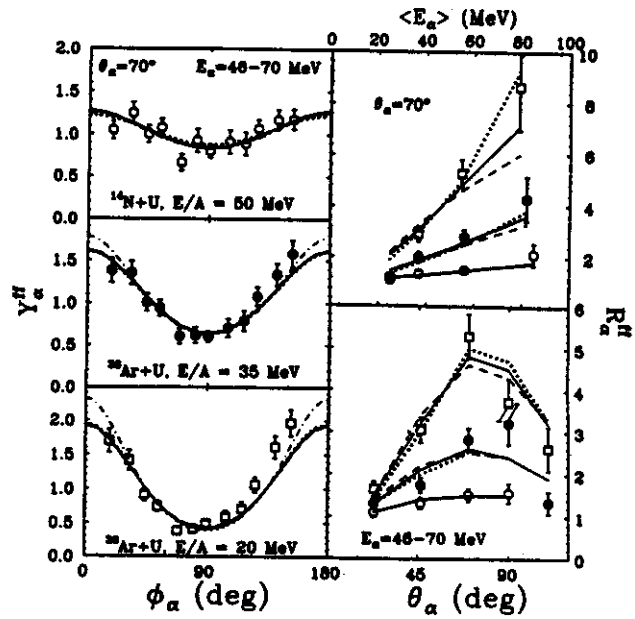

Fig. 1. Left hand panels: Azimuthal distributions, between fission fragments and α-particles for E_α=46-70 MeV and θ_α=70°. Right hand panels: In-plane over out-of-plane ratio for coincident fission fragments and α-particles. The top panel shows the dependence of the ratio on the kinetic energy of α-particles emitted at θ_α=70°; the bottom panel shows the dependence of the ratio on the emission angle for α-particles with E_α=46-70 MeV. The solid, dashed, dotted, and dot-dashed lines depict calculations described in the text.

such fits are shown by the dot-dashed curves in the left hand panels of Fig. 1. The extracted anisotropies are shown on the right hand side of Fig. 1, as a function of α-particle kinetic energy, $\langle E_\alpha \rangle$, for θ_α=70° (top panel), and as a function of emission angle, θ_α, for E_α=46-70 MeV (bottom panel). The most pronounced azimuthal asymmetries are observed for high energy α-particles emitted at θ_α=70°-90°. The enhanced emission of α-particles in the fission plane becomes less pronounced with increasing projectile velocity.

Decreasing values of R_α^{ff} correspond to less enhanced emission in the entrance channel reaction plane, for fission fragments, α-particles, or both. In order to assess the degree to which emission is enhanced in the entrance channel reaction plane, we assumed that the measured azimuthal correlations result from a convolution of the individual emission patterns of α-particles and fission fragments. The two emission patterns were described with respect to the orientation of the entrance channel reaction plane and parametrized as in Refs. 3,4. These parametrizations, given below, are chosen because of their simplicity and because they can fit the experimental data rather well. Different functional forms are not expected to change our qualitative conclusions.

The probability distribution, $P(\phi)$, for the angle ϕ between the entrance channel scattering plane and the fission plane was parametrized as.[3]

$$P_f(\phi) \propto \exp[-C\sin^2\phi] \quad . \qquad (1)$$

Since C cannot be determined a priori, C is treated as an adjustable parameter.

The emission of α-particles was described using an expression for the emission from an ideal gas of temperature T, rotating with angular velocity $\vec{\omega}$ perpendicular to the reaction plane, and moving with a velocity v_o parallel to the beam axis[3,4]:

$$P_\alpha(E_\alpha,\theta_\alpha,\phi_\alpha-\phi) \propto$$

$$\sqrt{(E_\alpha-V_c)E_s}\ \frac{J_1(iK)}{iK}\ \exp[-E_s/T] \qquad (2)$$

Here, $E_s=E_\alpha-V_c+E_o-2\sqrt{E_o(E_\alpha-V_c)}\cos\theta_\alpha$, $K=\frac{R}{T}\omega\sqrt{2m_\alpha[E_s-(E_\alpha-V_c)\sin^2\theta_\alpha\sin^2(\phi_\alpha-\phi)]}$, and $E_o=.5m_\alpha v_o^2$; J_1 denotes the first-order Bessel function; E_α, m_α, θ_α and ϕ_α are the energy, mass, polar and azimuthal angles of the emitted particle; the parameter V_c corrects for Coulomb repulsion from the heavy reaction residue, assumed to be at rest in the laboratory[4]. For comparison to measurements, one must sum over all possible orientations of the reaction plane[3]. Accordingly, the correlations between coincident fission fragments and α-particles are given by:

$$Y_\alpha^{ff}(E_\alpha,\theta_\alpha,\phi_\alpha) \propto \int_0^{2\pi} d\phi\ P_f(\phi)\ P_\alpha(E_\alpha,\theta_\alpha,\phi_\alpha-\phi) \quad . \qquad (3)$$

Three calculated correlations between α-particles and fission fragments, $Y_\alpha^{ff}(\phi_\alpha)$, are shown by the solid, dashed, and dotted curves in the left hand panels of Fig. 1. The parameters used for these calculations are listed in Table 1. The results of these calculations are nearly indistinguishable. Considerable ambiguities remain concerning the individual α-particle and fission fragment azimuthal distributions because wider fission distributions, $P_f(\phi)$, can be compensated by narrower α-particle distributions, $P_\alpha(E_\alpha,\theta_\alpha,\phi_\alpha-\phi)$, without significant effect on the α-fission correlation.

In order to reduce these ambiguities, one may explore the azimuthal correlation function for two α-particles detected in coincidence with two fission fragments. We have constructed averaged α-α azimuthal distributions, $\langle Y_{\alpha\alpha}^{ff}(\Delta\phi)\rangle$,

defined by:

$$\langle Y^{ff}_{\alpha\alpha}(\Delta\phi)\rangle \propto$$

$$\sum_{i\neq j} Y^{ff}_{\alpha\alpha}(\theta_1,\phi_i,\theta_2,\phi_j)\varepsilon_{ij}(\Delta\phi) \Big/ \sum_{i\neq j}\varepsilon_{ij}(\Delta\phi) \quad , \quad (4)$$

where $\varepsilon_{ij}(\Delta\phi)=1$ for $\Delta\phi=|\phi_i-\phi_j|\pm 30°$ and $\varepsilon_{ij}(\Delta\phi)=0$ otherwise; the function $\varepsilon_{ij}(\Delta\phi)$ selects only those detector pairs for which the difference in azimuthal angles lies within $\Delta\phi\pm 30°$. The summation in Eq. 4 is performed over all detectors i and j which are centered at polar angles $\theta_1=40°-50°$ and $\theta_2=60°-80°$, respectively. Averaged azimuthal α-α distributions, shown in Fig. 2, largely remove the parameter ambiguities which existed in the description of the α-fission correlations of Fig. 1. The dotted, dashed and solid curves represent calculations for the averaged azimuthal distributions using the same parameter values as in Fig. 1 and taking the individual detector locations into account according to Eq. 4. The solid curves in Figs. 1 and 2 represent calculations with an optimum choice of parameters. These calculations also reproduce other overall trends of the data rather well, including the energy and angular dependences shown by the solid lines in the right hand panels of Fig. 1.

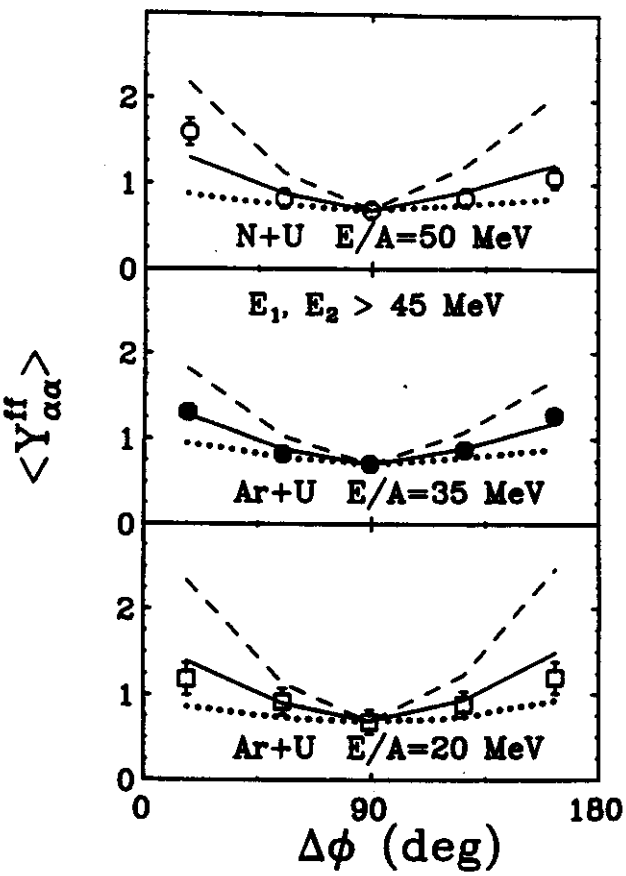

Fig. 2. Average azimuthal distributions of α-particles, $\langle Y^{ff}_{\alpha\alpha}\rangle$ (Eq. 4), for the reactions indicated. The solid, dashed and dotted lines depict calculations described in the text. Energy gates of E_1, E_2>45 MeV have been applied for all correlations shown.

Table 1: Parameters used for the calculations shown in Figs. 1-2.

Reaction	E/A	v_o/c†	T*	Rω/c	C	curve
$^{36}Ar+^{238}U$	20	0.08	4.0	0.04	4.8	dotted
$^{36}Ar+^{238}U$	"	"	"	0.05	3.0	solid
$^{36}Ar+^{238}U$	"	"	"	0.06	2.4	dashed
$^{36}Ar+^{238}U$	35	0.13	6.0	0.05	2.9	dotted
$^{36}Ar+^{238}U$	"	"	"	0.06	2.0	solid
$^{36}Ar+^{238}U$	"	"	"	0.07	1.8	dashed
$^{14}N+^{238}U$	50	0.16	7.5	0.05	1.6	dotted
$^{14}N+^{238}U$	"	"	"	0.065	1.1	solid
$^{14}N+^{238}U$	"	"	"	0.08	0.9	dashed

† Extracted from Ref. 9.
* In accordance with Ref. 4, this parameter was taken as 0.6 times the slope parameter extracted by a non-rotating moving source analysis of the kinetic energy spectrum of the emitted particle.

Additional insight can be gained by examining the distributions $P_f(\phi)$ and $P_\alpha(E_\alpha,\theta_\alpha,p)$, calculated from Eqs. 1 and 2 with the parameters which provide the best description of the experimental data. The α-

particle distribution has been calculated by setting θ_α=70°, and integrating Eq. 2 over the energies E_α=46-70 MeV. Fig. 3 show azimuthal distributions for α-particles (top) and fission fragments (bottom) calculated from the optimum parameters for the three reactions. Both fission and α-particle emission become less concentrated in the reaction plane as the projectile energy is increased. Emission out of the reaction plane appears to increase more rapidly for fission than for energetic α-particles. Such an energy dependence is expected from microscopic models which predict enhanced randomization of the particle momenta by nucleon-nucleon collisions at higher incident energies for which Pauli blocking becomes less effective.[5]

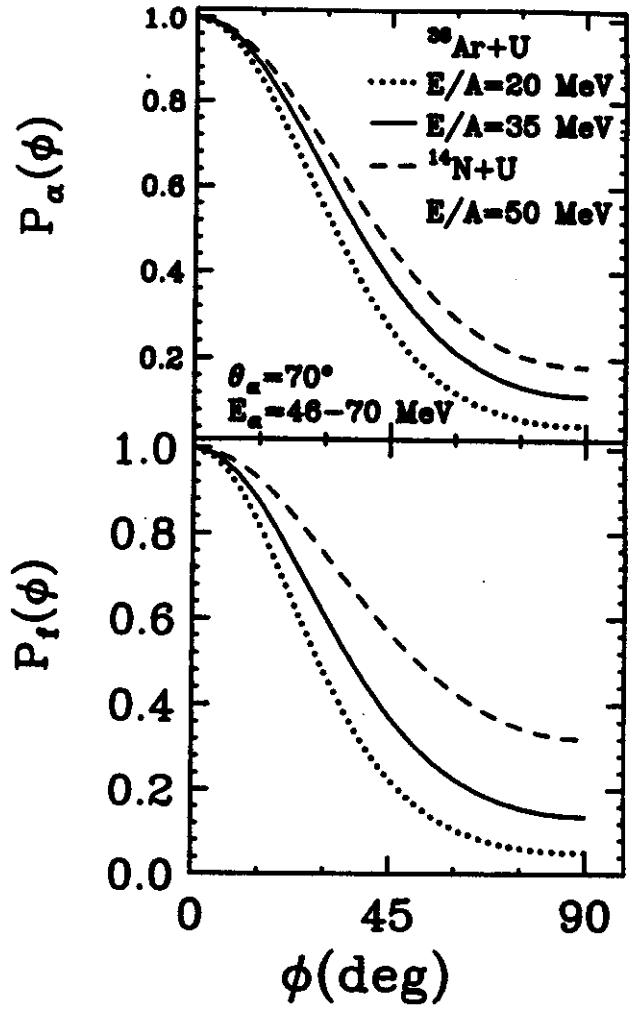

Fig. 3. Azimuthal distributions, defined with respect to the reaction plane and normalized to unity at φ=0°, calculated from Eqs. 1 and 2 with the optimum set of parameters for α-particles with E_α=46-70 MeV and θ_α=70° (top) and for fission fragments (bottom).

a. Department of Chemistry, Washington University, St. Louis, MS. 63130, USA

References

1. D.G. Sarantites et al., Nucl. Instr. and Meth. A264(1988)319; and D.W. Stracener et al., to be published in Nucl. Instr. and Meth.
2. A. Breskin, R. Chechik, Z. Fraenkel, P. Jacobs, I. Tserruya, and N. Zwang, Nucl. Instr. and Meth. 221(1984)363.
3. M.B. Tsang, D.J. Fields, C.K. Gelbke, D.R. Klesch, W.G. Lynch, K. Kwiatkowski, and V.E. Viola, Jr., Phys. Rev. Lett. 52(1984)1967.
4. M.B. Tsang et al., Phys. Lett. 148B, 265 (1984); C.B. Chitwood et al., Phys. Rev. C34(1986)858.
5. M.B. Tsang, G.F. Bertsch, W.G. Lynch, and M. Tohyama, Phys. Rev. C40(1989)1685.

AZIMUTHAL ASYMMETRY IN AR+V COLLISIONS FROM E/A=35 TO 85 MeV

W.K. Wilson, W. Benenson, D.A. Cebra, J. Clayton, S. Howden, J. Karn, T. Li, A. Nadasen[a], C.A. Ogilvie, A. Vander Molen, G.D. Westfall, J.S. Winfield and B. Young

Azimuthal distributions have proved useful in the study of reaction dynamics due to their sensitivity to collective motion.[1,2,3] In this report we review our studies of azimuthal anisotropy in the Ar+V system as a function of beam energy from E/A=35 to 85 MeV. Prior studies of azimuthal asymmetry at beam energies below E/A=100 MeV have focused on two-particle correlations;[1,2,4] we directly examine the azimuthal distributions relative to the measured reaction plane. At the lower beam energies studied, we find collective motion in the reaction plane manifested as an enhanced particle yield at azimuthal angles near the reaction plane. As the beam energy is increased, the azimuthal distributions tend towards isotropy, potentially yielding information about the changes in reaction dynamics over this transitional energy region.

The ^{40}Ar beams from E/A=35 to 85 MeV were produced by the K-500 and K-1200 cyclotrons at the NSCL in 10 MeV steps. To obtain a nearly symmetric system, ^{51}V was chosen as the target. Charged fragments were detected by the 170 phoswich telescopes of the MSU 4π Array.[5,6] A forward array of 45 phoswich telescopes was added, bringing the angular coverage to 85% of 4π sr. Angular, energy, and charge acceptances for the E/A=35 MeV data are detailed in Ref. 8. For the E/A=45 to 85 MeV data, the charge acceptance in the forward array was extended up to Z=18 and isotopic resolution in these detectors was dropped.

The method most commonly used to determine the reaction plane, introduced by Danielewicz and Odyniec,[7] depends on the presence of directed transverse momentum in the reaction plane. Since directed transverse momentum is weak for Ar+V in this energy range,[8,9] we have devised a new, more general, method which uses any in-plane enhancement to find the reaction plane. First, taking the p_z axis along the beam axis, we project the event onto the p_x-p_y plane. A line passing through the origin is then simultaneously fit to the (p_x,p_y) values for all of the particles. We take this line as the intersection of the reaction plane with the p_x-p_y plane. The reaction line (plane) is divided into two halves by the origin (beam axis). Next, we must establish which half of the reaction plane contains, or is closest to, the forward travelling projectile fragments. This is done by determining which half of our reaction line is closer to the projectile side of a reaction plane calculated using the global transverse momentum analysis of Danielewicz and Odyniec. The angle ϕ between a particle's projection into the p_x-p_y plane and the projectile side of the reaction line is then used to define the particle's azimuthal angle with respect to the reaction plane.

Auto-correlation is avoided by omitting the particle of interest from the event when calculating the reaction plane. Thus, the complete procedure for creating an azimuthal distribution function consists of three steps. First, the particle of interest is selected from the event. Next, the reaction plane is determined using the remaining particles. Finally, the azimuthal angle (ϕ) that the particle of interest makes with the projectile side of the reaction plane is calculated. This entire procedure, including the reaction plane calculation, is repeated for each particle of interest in the event.

The reaction plane found using the new

technique was compared on an event by event basis with the reaction plane calculated with the method of Danielewicz and Odyniec. A plot of the differences between the two planes displays a peak centered on 0°. The new technique gives a somewhat stronger in-plane enhancement than the method of Danielewicz and Odyniec for our data, indicating a more accurate calculation of the reaction plane; however, both techniques give qualitatively similar results. As a check, we took random particles from different data events to create test events with no correlations, and used the new technique to search for any spurious azimuthal asymmetry. This verified that the major features of our results are not due to the technique or to detector biases.

In Fig. 1 we show the magnitude of the in-plane enhancement found in the E/A=35 MeV data for Z=1 fragments, gated on the rapidity region in which the enhancement is strongest, y less than y_{cm}. The ϕ distribution peaks on the projectile and target sides of the reaction plane, 0° and 180° respectively. To quantify this enhancement, we introduce two new parameters: F_{ip} and F_{ps}. The first parameter is the fraction of particles emitted "in plane" (within 45° of the reaction plane) and the second is the fraction of particles emitted on the "projectile side" (within 90° of the projectile side of the reaction plane). These quantities are determined by the gates shown in Fig. 1 and are calculated from the ratios of counts found in the gates to the total numbers of counts. Azimuthally isotropic emission would correspond to both fractions equaling 0.5. For reference, the data in Fig. 1 have F_{ip}=0.553 ±0.0002 and F_{ps}=0.480±0.002.

The azimuthal distributions may now be studied as a function of the rapidity in the lab frame, allowing us to distinguish between some of the possible mechanisms that could be causing the asymmetry. For example, directed transverse

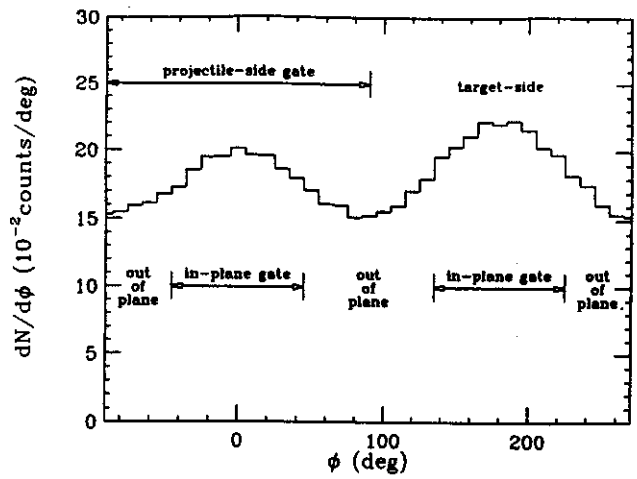

Fig. 1. The ϕ distribution of H emitted at low rapidity ($y \leq y_{cm}$) from the reaction E/A=35 MeV Ar+V. We define ϕ as the azimuthal angle with respect to the reaction plane, and $dN/d\phi$ as the number of particles found at each ϕ. The projectile-side and in-plane gates, shown in this figure by arrows, are used to produce the results show in Fig. 2.

momentum would lead to enhanced emission on the target side at low rapidity and on the projectile side at high rapidity. This emission pattern would cause F_{ps} to rise as a function of rapidity, going through 0.5 at $y=y_{cm}$. On the other hand, rotation of a midrapidity source around an axis perpendicular to the reaction plane would result in a F_{ps}=0.5 for all rapidities, while F_{ip} would show enhanced particle emission in the reaction plane around $y=y_{cm}$.

The azimuthal fraction for Z=1 and 2 fragments produced in E/A=35 MeV reactions are shown in Fig. 2. We find that F_{ps} is less than 0.5 at low rapidities and greater than 0.5 at high rapidities, indicating the presence of directed transverse momentum. This pattern is to be expected, since directed collective motion has been observed before in this system.[8,9] Note that the effect is stronger for He than for H, also in agreement with the previous results.

The largest F_{ip} values occur at rapidities near and below y_{cm}, where the azimuthal distribution is characterized by a simultaneous

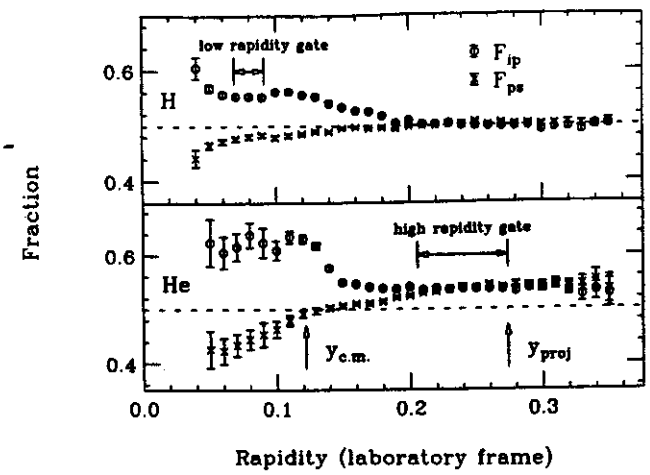

Fig. 2. The lab-rapidity dependence of the azimuthal asymmetry exhibited by H and He produced in the reaction E/A=35 MeV Ar+V. F_{ip} and F_{ps} are defined in the text. Azimuthally isotropic emission is shown with the dashed lines. The rapidity gates are used to produce the results shown in Fig 3.

enhancement on both the projectile and target sides, similar to that expected for rotational collective motion (see Fig. 2). This is distinct from the directed transverse momentum enhancement, which only contributes to the target side in this rapidity region. As the rapidity increases, the azimuthal asymmetry decreases to a constant value. For He at high rapidities, the in-plane enhancement is almost all on the projectile side, indicating that the F_{ip} asymmetry is dominated by directed transverse momentum in this region. The in-plane enhancement at each rapidity is stronger for He than for H.

To compare data at different beam energies, we place two rapidity gates on $F_{ip}(y)$. As shown in Fig. 2, the first gate is place at low rapidity where the asymmetry is strongest ($y_{proj}/4 \leq y \leq y_{proj}/3$). The second is placed at high rapidity where the azimuthal asymmetry is dominated by the directed transverse momentum component of the collective motion ($3y_{proj}/4 \leq y \leq y_{proj}$). Figure 3 shows that both components of the azimuthal asymmetry decrease as the beam energy is increased. At high rapidities, F_{ip} is consistent with isotropic emission for E/A near 75 to 85 MeV. Our technique does not cause this trend by losing its sensitivity to the reaction plane for the higher energy data. Simulations show that, given equal amounts of in-plane enhancement, the most critical factor in determining the reaction plane is the multiplicity, which in fact slightly increases with E_{beam}.

The data for the lowest beam energy agree qualitatively with measurements by Chitwood et al. of two-particle correlation functions for E/A=25 MeV O+Au.[2] They found peaks in the correlation functions at $\Delta\phi$=0° and 180°, consistent with preferential in-plane emission. Our azimuthal distributions support the identification of the symmetry plane in the two-particle correlations with the reaction plane. The correlations were interpreted by Chitwood et al. in terms of a model incorporating the decay of a rotating source, which predicts that the asymmetry should increase with the mass of the detected particle and the angle with respect to the beam axis. Our F_{ip} observations are also in general agreement with these rotating source predictions.

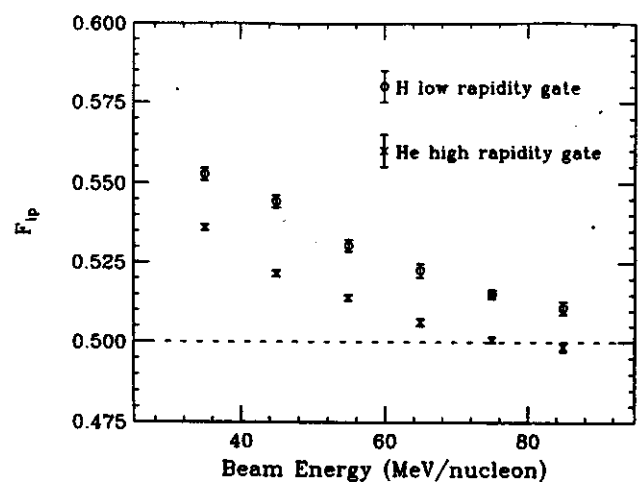

Fig. 3. The beam energy dependence of the azimuthal asymmetry for light particles produced in Ar+V reactions. The dashed line corresponds to azimuthally isotropic emission.

To summarize, we observe collective motion at the lower beam energies, perhaps due to rotation in the participant zone, causing particles to be preferentially emitted near the reaction plane on both the target and projectile sides. This motion creates an azimuthal asymmetry which is distinct from and stronger than that due to directed transverse momentum for this system. As the beam energy is increased from E/A=35 to 85 MeV, the reaction dynamics appear to change, and both forms of collective motion decrease for light particles. There are several interesting routes of investigation to pursue in order to understand this change in dynamics. The F_{ps} asymmetry and - near the projectile rapidity - the F_{ip} asymmetry, are caused at least in part by directed transverse momentum, and analysis of the La+La system has shown that flow disappears at beam energies around E/A=30 to 50 MeV.[10] This disappearance has been interpreted as a balancing of the attractive and repulsive components of the nuclear mean field. As for F_{ip} at lower rapidities, if rotation is causing the majority of this in-plane enhancement, then we would expect the effect to be sensitive to the lifetime of the source. Perhaps the speculated onset of simultaneous multifragmentation at the higher energies inhibits the establishment of a rotating source by shortening the lifetime of the system.

---

a. University of Michigan, Dearborn

References

1. M.B. Tsang, W.G. Lynch, C.B. Chitwood, D.J. Fields, D.R. Klesch, C.K. Gelbke, G.R. Young, T.C. Awes, R.L. Ferguson, F.E. Obenshain, F. Plasil and R.L. Robinson, Phys. Lett. 148B(1984)265.
2. C.B. Chitwood, D.J. Fields, C.K. Gelbke, D.R. Klesch, W.G. Lynch, M.B. Tsang, T.C. Awes, R.L. Ferguson, F.E. Obenshain, F. Plasil, R.L. Robinson and G.R. Young, Phys. Rev. C34(1986)858.
3. K.G.R. Doss, H.-A. Gustafsson, H. Gutbrod, J.W. Harris, B.V. Jacak, K.-H. Kampert, B. Kolb, A.M. Poskanzer, H.-G. Ritter, H.R. Schmidt, L. Teitelbaum, M. Tincknell, S. Weiss and H. Wieman, Phys. Rev. Lett. 59(1987)2720.
4. H.J. Rabe, K.D. Hildenbrand, U. Lynen, W.F.J. Müller, H. Sann, H. Stelzer, W. Trautmann, R. Trockel, R. Wada, J. Pochodzalla, E. Eckert, P. Kreutz, A. Kühmichel, N. Brummund, R. Glasow, K.H. Kampert, R. Santo and D. Pelte, Phys. Lett. 196B(1987)439.
5. G.D. Westfall, J.E. Yurkon, J. Van der Plicht, Z.M. Koenig, B.V. Jacak, R. Fox, G.M. Crawley, M.R. Maier and B.E. Hasselquist, Nucl. Instr. and Meth. A238(1985)347.
6. C.A. Ogilvie, D.A. Cebra, J. Clayton, S. Howden, J. Karn, A. Vander Molen, G.D. Westfall, W.K. Wilson and J.S. Winfield, Phys. Rev. C40(1989)654.
7. P. Danielewicz and G. Odyniec, Phys. Lett. 157B(1985)146.
8. C.A. Ogilvie, D.A. Cebra, J. Clayton, P. Danielewicz, S. Howden, J. Karn, A. Nadasen, A. Vander Molen, G.D. Westfall, W.K. Wilson and J.S. Winfield, Phys. Rev. C40(1989)2592.
9. C.A. Ogilvie, D.A. Cebra, J. Clayton, P. Danielewicz, S. Howden, J. Karn, A. Nadasen, A. Vander Molen, G.D. Westfall, W.K. Wilson and J.S. Winfield, Phys. Lett. 231B(1989)35.
10. D. Krofcheck, W. Bauer, G.M. Crawley, C. Djalali, S. Howden, C.A. Ogilvie, A. Vander Molen, G.D. Westfall, W.K. Wilson, R.S. Tickle and C. Gale, Phys. Rev. Lett. 63(1989)2028.

REACTION PLANE DETERMINATION

B.M. Young, W.K. Wilson, W. Benenson, C.A. Ogilvie, G.D. Westfall

Recent investigations of transverse and rotational collective motion in heavy ion collisions have focused on the azimuthal distributions of emitted fragments relative to the reaction plane.[1,2] The method for reaction plane determination, introduced by Danielewicz and Odyniec[3] specifically for observing directed transverse momentum, is insensitive to other effects, such as fragment emission from a rotating source, which could also give rise to a reaction plane. To facilitate analysis of systems where directed transverse momentum is weak, we have developed a new method for reaction plane determination which is sensitive to any in-plane enhancement.

If the p^z axis is taken along the beam axis (Fig. 1) then a reaction plane would intersect the p^x-p^y plane in a line passing through the origin (p^x=p^y=0). Using this fact, the reaction plane for a given event is found by fitting such a line (p^y=bp^x) to the perpendicular momenta (p_i^x,p_i^y) of all the particles in the event. This is done by minimizing with respect to b the sum of the perpendicular distances d_i between the line and the points (p_i^x,p_i^y).

Any method for determining reaction planes should exhibit no azimuthal preferences, that is, the distribution of reaction planes found for many events should be isotropic.To test this, simulated events with in-plane enhancement and directed transverse momentum were filtered through a software model of the MSU 4π array. For each event the reaction plane was found using the above technique. The resulting histogram of the calculated plane angles shows a slight periodic anisotropy. This is due to the finite size of the elements in the array, which establishes a preference for finding reaction planes at the same angles where the detector elements are located.

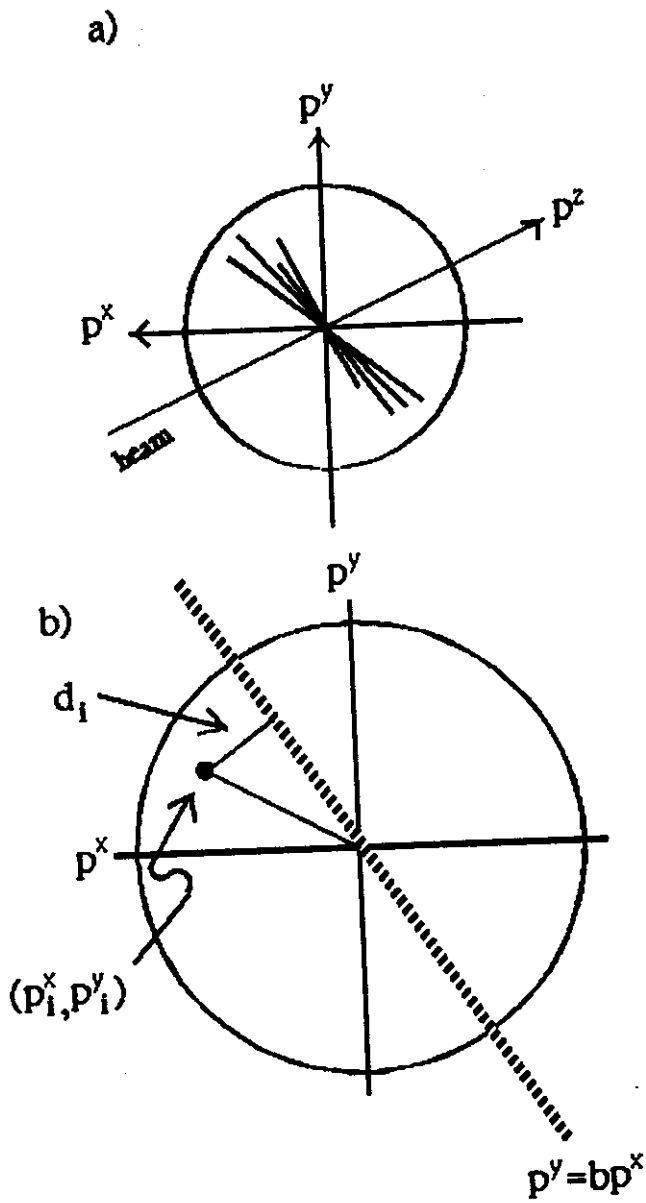

Fig. 1. a) Geometry for reaction plane determination. b) Reaction plane is found by summing d_i for all particles in event and minimizing with respect to b.

For events with directed transverse momentum, Danielewicz and Odyniec[3] define a vector Q in the p^x-p^y plane

$$Q = \sum_i \omega_i p_i^t$$

where

$$\omega_i = p_i^{z,cm}/|p_i^{z,cm}|$$

$$p_i^t = (p_i^x, p_i^y)$$

The direction of Q defines the projectile (forward-going in the c.m.) side of the reaction plane. Since the reaction plane found by our method is divided into two halves by the origin of the p^x-p^y plane, the half which lies closer to Q corresponds to the projectile side. Thus we can make a direct comparison between our method and that of Danielewicz and Odyniec. Simulations of events with different amounts of directed transverse momentum and in-plane enhancement show that our method is able to detect reaction planes with slightly better accuracy than the traditional method. It has been pointed out[2] that since our technique is sensitive only to the in-plane enhancement, it is possible that an out-of-plane squeeze-out effect could lead to significant error in the found reaction plane. As a check, the reaction planes found from the two methods were compared on an event by event basis for Ar+V data taken at beam energies between 35 and 85 MeV/A. The resulting histogram for 85 MeV/A, shown in Fig. 2, displays a peak centered at 0° indicating that the two techniques usually find reaction planes with similar azimuthal orientations. This implies that squeeze-out, which becomes more prevalent at higher beam energies, does not present a problem for our method at MSU energies.

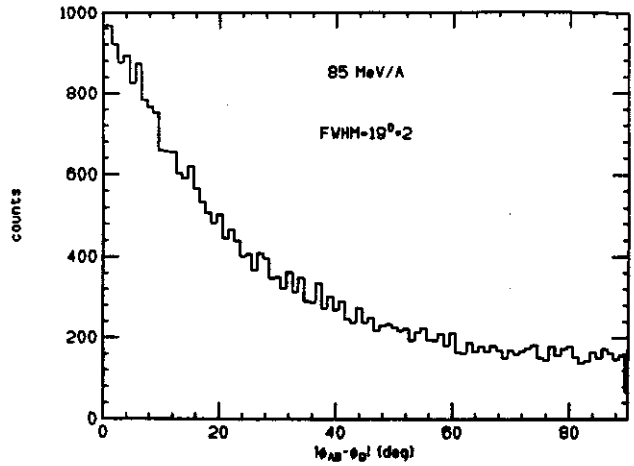

Fig. 2 Comparison of reaction plane angles found using our method (ϕ_{AB}) and that of Danielewicz and Odyniec (ϕ_Q).

References

1. C.A. Ogilvie, W. Bauer, D.A. Cebra, J. Clayton, S. Howden, and J. Karn, A. Nadasen, A. Vander Molen, G.D. Westfall, W.K. Wilson, and J.S. Winfield, submitted to Phys. Rev. C Rap. Comm. (1990).
2. W.K. Wilson, W. Benenson, D.A. Cebra, J. Clayton, S. Howden, J. Karn, T. Li, C.A. Ogilvie, A. Vander Molen, G.D. Westfall, J.S. Winfield, and B. Young, submitted to Phys. Rev. C Rap. Comm. (1990).
3. P. Danielewicz and G. Odyniec, Phys. Lett. 157B,146(1985).

THE DISAPPEARANCE OF FLOW AND ITS RELEVANCE TO NUCLEAR MATTER PHYSICS

C.A. Ogilvie[a], W. Bauer, D.A. Cebra, J. Clayton, S. Howden, J. Karn, A. Nadasen[b], A. Vander Molen, G.D. Westfall, W.K. Wilson and J.S. Winfield

Recently Krofcheck et al.[1] reported the disappearance of transverse momentum flow in an excitation function of La+La collisions at intermediate energy. At high beam energies, the observed collective motion[2] towards positive scattering angles is thought to be generated by compressed nuclear matter that was formed in the early stages of the reaction. At lower beam energies, directed collective motion has been observed[3] and attributed to the attractive mean-field which deflects the fragments to negative scattering angles[4]. The balancing between these two dynamic effects at a beam energy of $E_{balance}$, i.e. the disappearance of flow, may elucidate the role of compression in these collisions.

It is known that the value of the nuclear compressibility (K) and the in-medium nucleon-nucleon cross section both affect the build-up of compression at intermediate beam energies. However, there is substantial uncertainty in the actual value of K and in the manner in which the in-medium cross section differs from the free nucleon-nucleon cross-section. In this work we present a measurement of $E_{balance}$ for the Ar+V reaction and then investigate whether this can provide information on K and the in-medium cross-section.

We have measured the production of charged light fragments from the reaction Ar+V using beam energies of 35 to 85 MeV/nucleon in 10 MeV/nucleon steps. The fragments were detected with the phoswich detectors in the MSU 4π array. Central collisions were selected from the data using the measured mid-rapidity charge as an impact parameter filter[5]. The reaction plane was determined[6] and the deduced perpendicular momenta were rescaled to correct for the effects of momentum conservation as in Ref. 3.

In Fig. 1 we present the bombarding energy dependence of the slope through mid-rapidity of the fractional in-plane transverse momentum for the light fragments. At a given bombarding energy, the collective motion appears to increase with the mass of the emitted fragment. Above 45 MeV/nucleon there is a clear decrease in the magnitude of the collective motion. Because the observed collective motion is consistent with zero near the highest bombarding energy, we can establish a lower limit on $E_{balance}$. We find that $E_{balance} \geq 76$ MeV/nucleon. Also, the data indicates that $E_{balance}$ may be the same for different mass fragments. This is a necessary condition before comparisons can be made to theoretical models that do not produce fragments.

We have also performed calculations using the Boltzman-Uehling-Uhlenbeck (BUU) model to study the effects of the in-medium cross section and K on $E_{balance}$. The results of the calculations are summarized in Table I, where we list $E_{balance}$ for different values of K and independent medium cross sections. The results of the calculations suggest that $E_{balance}$ is strongly dependent on the in-medium cross-section and weakly dependent on the nuclear

Table I: Calculated $E_{balance}$ values for Ar + V colloisions with different parameter sets of the BUU model. R is the ratio of the in-medium nucleon-nucleon scattering cross-section to the free nucleon-nucleon scattering cross section.

K (MeV)	R	$E_{balance}$ (MeV/nuclon)
200	1.0	80
380	1.0	88
200	0.9	96
200	0.8	108
200	0.7	122

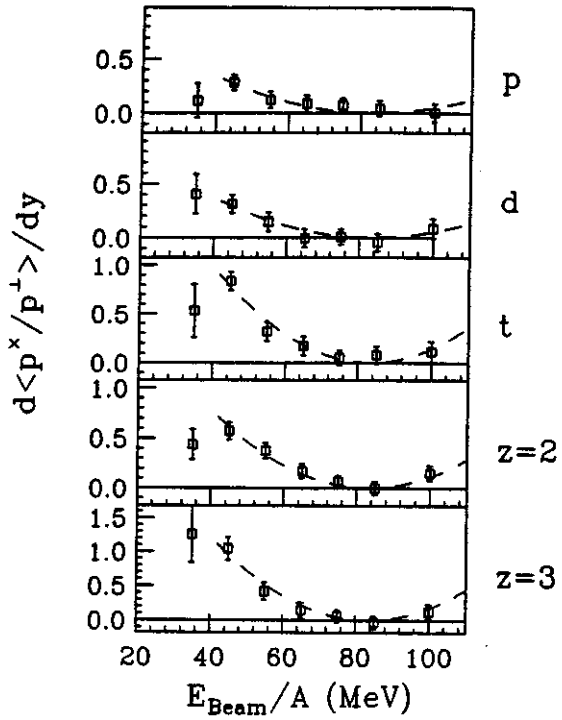

Fig. 1. The excitation functions of the measured flow for different fragments emitted in Ar+V central collisions. The dashed line corresponds to an optimal fit for a parabolic line shape.

compressability. Definitive constraints on these quantities must wait for both upper and lower limits on $E_{balance}$, as well as for the inclusion of Coulomb effects, momentum dependent interactions and a better understanding of the surface term in the nuclear interaction. Finally, it is worth noting that Ref. 1 reported $E_{balance} \leq 50$ MeV/nucleon for the La+La system. It is possible that the measured mass dependence of $E_{balance}$ may provide independent constraints on the values of the in-medium cross-section and the nuclear compressibility.

---

a. present address, GSI
b. University of Michigan, Dearborn

References

1. D. Krofcheck et al., Phys. Rev. Lett. 63(1989)2028.
2. K.G. Doss et al., Phys. Rev. Lett. 59(1987)2720.
3. C.A. Ogilvie et al., Phys. Rev. C40(1989)2592.
4. M.B. Tsang et al., Phys. Rev. Lett. 57(1986)559.
5. C.A. Ogilvie et al., Phys. Rev. C40(1989)654.
6. W.K. Wilson et al., submitted to Phys. Rev. C (1990).

SYSTEMATIC BEHAVIOR OF THE DISAPPEARANCE OF FLOW IN HEAVY-ION COLLISIONS

D. Krofcheck, G.M. Crawley, C. Djalali[a], S. Howden, C.A. Ogilvie[b], A. Vander Molen, G.D. Westfall, W.K. Wilson and R.S. Tickle[c]

The recently observed[1,2] phenomenon of the vanishing of collective, directed transverse momentum, known colloquially as the 'disappearance of flow', may provide information on the build-up of pressure during the early stages of heavy-ion collisions. This is important because the pressure build-up may be related to the nuclear compressibility. If the energy needed to squeeze nuclear matter is plotted versus the nuclear density, then knowledge of the nuclear compressibility would determine the shape of the curve in the high density region ($\rho \geq 2\rho_0$) of the nuclear equation-of-state. Regions of lower density are essentially fixed by the properties of ground state nuclear matter.

It is believed that the pressure build-up can be studied by determining the beam energy at which attractive and repulsive scatterings are in rough equilibrium, defined here as $E_{balance}$, for a variety of beam and target combinations. $E_{balance}$ should exhibit a mass dependence because the repulsive scattering from the pressure build-up is proportional to the volume of the overlap region (A of the target or projectile in a symmetric system). The balancing force from attractive scattering is proportional to the surface area of the overlap region ($A^{2/3}$ dependence). The measured values of $E_{balance}$ for a variety of systems can then be compared directly to the results of Boltzmann-Uehling-Uhlenbeck (BUU) calculations which incorporate the nuclear compressibility and the nucleon-nucleon (NN) scattering cross section.

A start on the mass systematics of $E_{balance}$ has already been achieved using the systems[1,2] La+La and Ar+V. We report here on the disappearance of flow for the Nb+Nb system. Digitized pictures of hardware-selected central collisions from the Nb+Nb reaction at incident energies of 60 and 120 MeV/nucleon were obtained at the Lawrence Berkeley Laboratory Streamer Chamber Facility using charge-coupled device (CCD) cameras[3]. The pictures were analyzed with fully automated data analysis techniques[4] and the final data sets consisted of 280 events at 60 MeV/nucleon and 380 events at 120 MeV/nucleon. The median multiplicities of reconstructed tracks for mass≤4 fragments were 16 and 20 for 60 and 120 MeV/nucleon, respectively. The average in-plane transverse momentum (TM) spectra were then obtained using the techniques of Danielewicz and Odyniec[5]. Figs. 1-2 show these spectra for the two beam energies. These curves are asymmetric about mid-rapidity due to low energy thresholds and limitations in the automated analysis software. As in the previous streamer chamber work, the average value of TM in the forward hemisphere is used to characterize the flow as (3±5) MeV/c at E_{beam}=60 MeV/nucleon and (12±5) MeV/c at E_{beam}=120 MeV/nucleon. These values are not

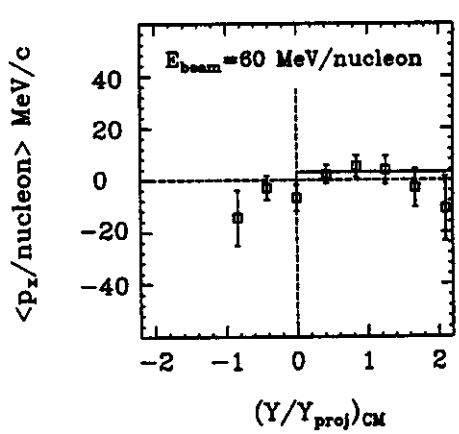

Fig. 1. The average in-plane transverse momentum for the Nb+Nb reaction at E_{beam}=60 MeV/nucleon. The solid line indicates the average in-plane transverse momentum near the projectile rapidity.

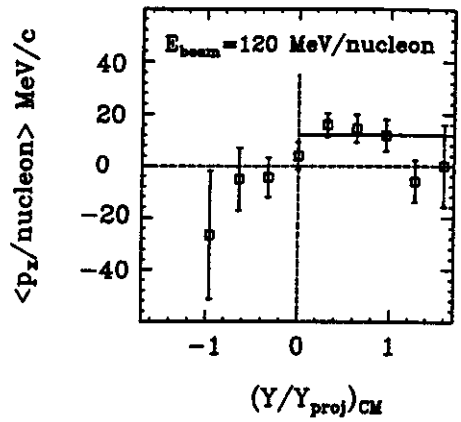

Fig. 2. Same as in Fig. 1, except that E_{beam}=120 MeV/nucleon.

corrected for the dispersion of the empirically determined reaction plane about the true reaction plane. The present results can also be compared to higher energy Nb+Nb results obtained by the plastic ball group[6]. Re-defining flow as the slope of the TM curves in Figs. 1-2 at mid-rapidity and following the analysis techniques in Ref. 6, we obtain the results presented in Fig. 3.

In Table I, we present indications of a possible $E_{balance}$ mass dependence. The lighter mass Ar+V system has the largest apparent $E_{balance}$ value while the heavier La+La system has the lowest apparent value. The present

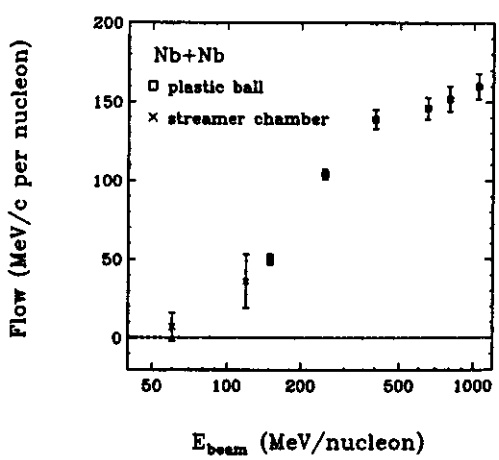

Fig. 3. The present data acquired with the streamer chamber compared to previous results obtained at higher bombarding energies with the plastic ball detector. The streamer chamber error bars include uncertainties from statistics, experimental systematics and fitting a line through the mid-rapidity region.

Table I: Approximate $E_{balance}$ for several systems.

System	$E_{balance}$(MeV/nucleon)
Ar+V	≥76
Nb+Nb	~60
La+La	≤50

result seems to fall somewhere in between the two, but further measurements of the TM excitation function for Nb+Nb at intermediate beam energies are needed before any definitive statements can be made.

a. University of South Carolina
b. Present address, GSI
c. University of Michigan

References

1. D. Krofcheck et al., Phys. Rev. Lett. 63(1989)2028.
2. C.A. Ogilvie et al., submitted to Phys. Rev C. (January, 1990).
3. S.P. Angius et al., Nucl. Instr. and Meth. A273(1987)283.
4. D. Krofcheck et al., Nucl. Instr and Meth. (in press).
5. P. Danielewicz and G. Odyniec, Phys. Lett. 157B(1985)146.
6. H. Gutbrod, A. Poskanzer and H.G. Ritter, submitted to Repts. Prog. in Phys. (March, 1989).

TWO-PROTON CORRELATION FUNCTIONS FOR EQUILIBRIUM AND NON-EQUILIBRIUM EMISSION

W.G. Gong, C.K. Gelbke, N. Carlin,[a] R.T. DeSouza, Y.D. Kim, W.G. Lynch, T. Murakami,[b] G. Poggi,[c] D. Sanderson, M.B. Tsang, H.M. Xu, D.E. Fields,[d] K. Kwiatkowski,[d] R. Planeta,[d] V.E. Viola, Jr.,[d] S.J. Yennello,[d] and S. Pratt[e]

Two protons, emitted at small relative momenta from an excited nuclear system, carry information about the space-time characteristics of the emitting source.[1-10] The shape of the two-proton correlation function reflects the interplay of the short-range nuclear interaction, the Pauli exclusion principle, and the long range Coulomb interaction between the two emitted protons. The short range nuclear interaction is dominated by the attractive singlet S-wave interaction which leads to a pronounced maximum in the two-proton correlation function at relative momentum q≈20 MeV/c, when the average distance upon emission is of the order of 10 fm or less. The long range Coulomb interaction as well as the Pauli exclusion principle produce a minimum at q=0. Some directional information is provided by antisymmetrization effects[1,7,8] which are important when $|\vec{q}\vec{r}|<h$, where $\vec{q}$ and $\vec{r}$ denote the relative momentum and position vectors upon emission.

The average distance between the two coincident protons upon emission depends on the spatial dimension, d, of the emitting system and on the time interval, τ, between the two emission processes; it is of the order of $d+\bar{v}\tau$, where $\bar{v}$ is the average velocity of the emitted particles. For the decay of equilibrated compound nuclei with temperatures below 5 MeV, estimated emission times are larger than several hundred fm/c.[11] As a consequence, the average distance between emitted particles is much larger than the size of the emitting nucleus and the effects of the Coulomb interaction and the Pauli principle should dominate. On the other hand, preequilibrium light particle emission in intermediate energy heavy ion collisions is calculated to proceed on much shorter time scales[12,13] and average particle separations may reflect the spatial dimension of the emitting system rather than the emission rate. Here, the nuclear interaction should be prominent.

We have performed a comparative study of two-proton correlation functions measured for preequilibrium and equilibrium emission processes. Preequilibrium emission was studied in "forward kinematics" for the reaction $^{14}N+^{197}Au$ at E/A=75 MeV. Equilibrium emission was studied, at E/A=31 MeV, in "reverse kinematics" for the reaction $^{129}Xe+^{27}Al$ and for the nearly-symmetric system $^{129}Xe+^{122}Sn$. Light particles were detected with two ΔE-E detector arrays consisting of 300-400 μm thick silicon ΔE-detectors and 10 cm long NaI(Tl) or CsI(Tl) E-detectors. An array consisting of 37 Si-CsI(Tl) telescopes[14] was centered at the polar and azimuthal angles of θ=25° and φ=0°; its detectors had solid angles of ΔΩ=0.37 msr and a nearest neighbor spacing of Δθ=2.6°. Another array consisting of 13 Si-NaI(Tl) telescopes was centered at θ=25° and φ=90°; its detectors had solid angles of ΔΩ=0.5 msr and nearest neighbor spacings of Δθ=4.4°. Downscaled singles and coincidences were taken simultaneously. Energy calibrations are accurate to better than 2%.

Two-proton correlation functions measured for the $^{14}N+^{197}Au$ reaction are shown in Fig. 1. A strong dependence on the total laboratory momentum, P, of the coincident proton pair is measured, consistent with previous observations.[2-6,8] The solid curves show theoretical correlation functions predicted for sources of Gaussian density, $\rho(r)\propto\exp(-r^2/r_o^2)$,

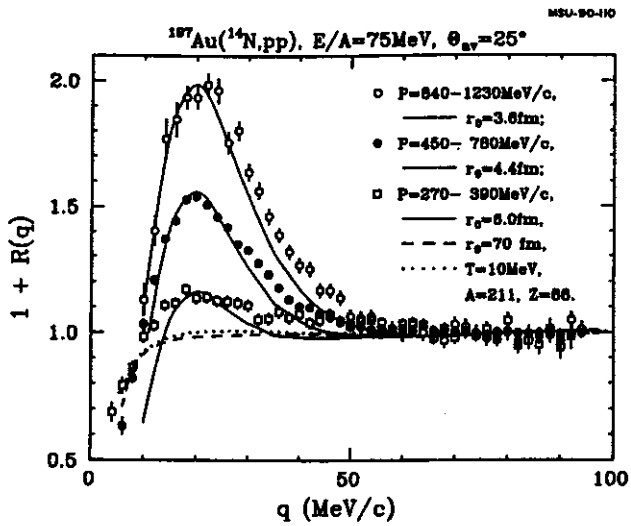

Fig. 1. Two-proton correlation functions measured for the $^{14}N+^{197}Au$ reaction at E/A=75 MeV for the indicated gates on the total momentum, P, of the two-proton pair. The solid and dashed curves show predictions for Gaussian sources of negligible lifetime and the dotted curve shows calculations for an evaporative source with the indicated parameters.

and negligible lifetime. Such calculations provide upper limits for the size of the emitting system. Since high energy protons detected in this reaction are emitted in rapid nonequilibrium processes, the neglect of temporal effects may be justifiable.[8] However, for small total momenta, the shape of the minimum at q≈0 can only be reproduced with sources of unphysically large dimensions, see the dashed curve. These correlations can be reproduced by assuming particle evaporation from a long lived equilibrated nucleus. Calculations assuming particle evaporation are indicated by the dotted curve and described in the discussion below.

Correlation functions measured for the $^{129}Xe+^{27}Al$ and $^{129}Xe+^{122}Sn$ reactions at E/A=35 MeV are shown in Fig. 2. They exhibit a minimum at q≈0, but no maximum at q≈20 MeV/c. Correlation functions of similar shape were reported for equilibrium emission in the $^{16}O+^{27}Al$[9] and $^{40}Ar+Ag$[10] reactions at E/A=8.75 and 44 MeV, respectively. The data shown in Fig. 2 correspond to proton energies slightly above the compound nucleus Coulomb barrier and

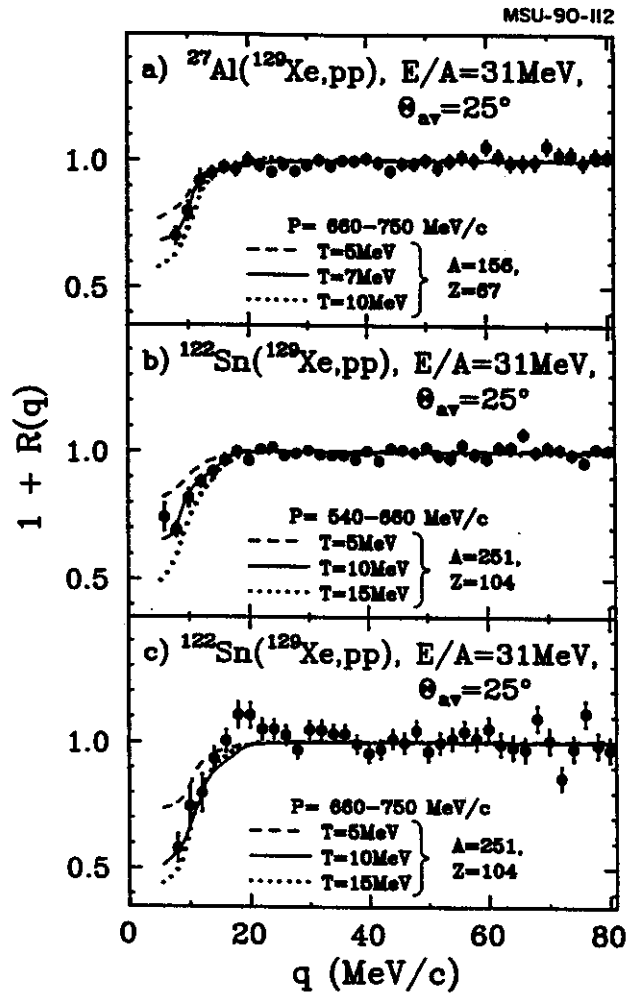

Fig. 2. Two-proton correlation functions measured for the $^{129}Xe+^{27}Al$ (part a) and $^{129}Xe+^{122}Sn$ (parts b,c) reactions at E/A=31 MeV for the indicated gates on the total momentum, P, of the two-proton pair. The curves represent calculations for evaporative sources with the parameters indicated.

are expected to be dominated by emission from long-lived equilibrated composite nuclei formed in incomplete fusion reactions. (For the $^{129}Xe+^{27}Al$ reaction, the total momentum gate P=660-750 MeV/c selects energies, in the center-of-mass frame of reference, E_{cm}≈15-23 MeV; for the $^{129}Xe+^{122}Sn$ reaction, the gates P=540-660 MeV/c and P=660-750 MeV/c select the energies E_{cm}≈15-27 MeV and E_{cm}≈27-40 MeV, respectively.)

Correlation functions for particle evaporation from long lived compound nuclei, can

be calculated by using the Wigner function formalism of Ref. 7. We have performed such calculations for the simple evaporative model of Ref. 11. The results, averaged over the appropriate momentum bin and folded with the resolution of the experimental apparatus, are shown by the dotted curve in Fig. 1 and the solid, dashed, and dotted curves in Fig. 2. The parameters used in these calculations, initial mass, A, charge, Z, and temperature, T, of the decaying nucleus, are indicated in the figures. Satisfactory agreement with the experimental data is obtained, indicating that the calculated emission rates have the correct order of magnitude.

---

a. University of São Paulo, São Paulo, Brazil
b. Kyoto University, Kyoto, Japan
c. University of Florence, Floence, Italy
d. Indiana University, Bloomington, IN 47405, USA
e. University of Wisconsin, Madison, WI 53706, USA

References

1. S.E. Koonin, Phys. Lett. 70B(1977)43.
2. W.G. Lynch et al., Phys. Rev. Lett. 51(1983)1850.
3. Z. Chen et al., Phys. Lett. B186(1987)280.
4. Z. Chen et al., Phys. Rev. C36(1987)2297.
5. J. Pochodzalla et al., Phys. Rev. C35(1987)1695.
6. J. Pochodzalla et al., Phys. Lett. B174(1986)36.
7. S. Pratt and M.B. Tsang, Phys. Rev. C36(1987)2390.
8. T.C. Awes et al., Phys. Rev. Lett. 61(1988)2665.
9. P.A. DeYoung et al., Phys. Rev. C39(1989)128.
10. D. Ardouin et al., University of Nantes, Internal Report LPN-89-02.
11. W.A. Friedman and W.G. Lynch, Phys. Rev. C28(1983)16.
12. J. Aichelin and G. Bertsch, Phys. Rev. C31(1985)1730.
13. W. Cassing, Z. Phys. A329(1988)471.
14. W.G. Gong, et al., Nucl. Instr. and Meth. A268(1988)190.

PROTON-PROTON CORRELATION FUNCTION IN ^{3}He + Ag REACTION AT E_{beam}=200MeV

F. Zhu, W.G. Lynch, T. Murakami, C.K. Gelbke, Y.D. Kim, T.K. Nayak, R. Pelak, M.B. Tsang, H.M. Xu
D.E. Fields[a], K. Kwiatkowski[a], R. Planeta[a], S. Rose[a], V. Viola[a], L.W. Woo[a],
S. Yennello,[a] J. Zhang[a]

Calculations suggest that proton-proton correlation functions at small relative angles can provide information about the space-time development of a nuclear collision.[1] Measurements[2,3] reveal that two particle correlation functions are larger for energetic particles. This suggest that the higher energy particles are emitted from a small source during the early stages of the reaction while the lower energy particles are emitted from more equilibrated source during the later stages of the reaction. Some sensitivity to the size of the projectile nucleus has also been observed in systematic comparisons between different systems. Indeed, smaller sources have been extracted for reactions with small projectiles and lager sources have been extracted from reactions with lager projectiles. In contrast, comparisons by Cebra et. al[4] between p + Ag and ^{14}N + Ag at E_{beam}=500MeV display no sensitivity to the projectile. They, however, did not explore the sensitivity of their measured correlations to the energy of the detected protons. To further investigate correlation functions with light projectiles, we measured two particle correlations for the ^{3}He + Ag reaction at E_{beam}=200MeV.

The experiment was performed at the Indiana University Cyclotron Facility. A 200MeV ^{3}He beam was used to bombard a natural Ag target of 1.05 mg/cm^2 areal density. two coincident light particles were detected with a high resolution hodoscope consisting of 13 closely packed telescopes.[5] Four of these telescopes, consisting of 75 μm,100 μm, 5mm, and 5mm silicon detectors, were used to detect particles with $1 \leq Z \leq 4$, and the other nine telescopes, consisting of 200 μm and 5mm silicon detectors followed by 10 cm NaI detector, were used to detect particles with Z=1,2. In front of each telescope there were two single wire gas counters which provide x and y position information which proved essential for reconstructing the relative momentum between the two detected particles.

The experimentally measured proton singles inclusive cross sections are shown in Fig. 1. During the experiment we put the hodoscope at two angles, one is forward at 40°, the other is backward at 110°. The lines correspond to moving source fits to these data. At the forward angles, there are two components to the spectra. At low energies, the rapidly decreasing part of the cross section is due to

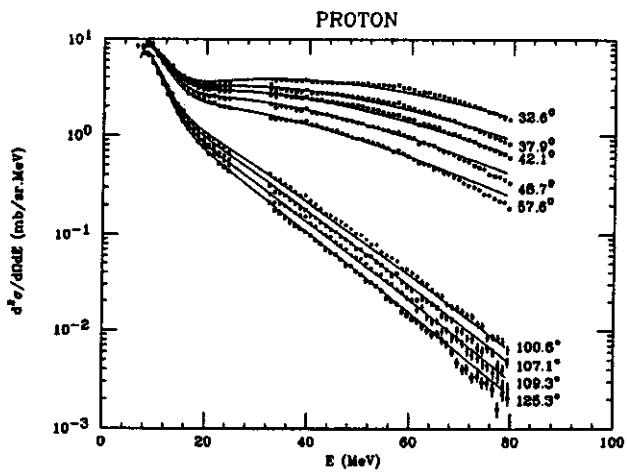

Fig. 1. Single particle inclusive cross sections of proton emitted in ^{3}He + Ag reaction at E_{beam} = 200 MeV at the Laboratory forward angles of 32.6°, 37.9°, 42.1°, 48.7°, 57.6° and backward angles of 100.6°, 107.1°, 109.3°, 125.3°. The curves are the moving source fits.

low energy protons emitted by an equilibrated or nearly equilibrated compound nucleus. At high energies one observes protons emitted by non-equilibrium emission mechanisms before the system get equilibrated. In the backward angles, this contribution from non-equilibrium emission gets less important and one observes mainly the emission from the equilibrated source.

Experimentally the correlation function R(q) is defined in terms of coincidence yield $Y_{12}(p_1,p_2)$ and the singles yield $Y_1(p_1)$ and $Y_2(p_2)$,

$$\sum Y_{12}(p_1,p_2)=C_{12}[1+R(q)]\sum Y_1(p_1)Y_2(p_2) \qquad (1)$$

Here, p_1 and p_2 are the momentum of the two particles in the lab frame and q is the relative momentum between the two particles. When two particles are emitted close to each other, their wave function of relative motion is modified by their mutual interactions through the nuclear and Coulomb potentials. Quantum statistical effects are also important for identical particles. With a greater spatial separation between the two emitted particles or at large relative momenta, these effects will become less important and the correlation functions vanishes. The normalization constant C_{12} in eq. (1) is therefore defined so that R(q) goes to zero for large relative momentum q where the final state interactions between the two particles vanish. The behavior of the experimental correlation functions at small relative momenta also contains the information about the space time extent of the emitting system. Theoretically if the time dependence of the emission process is neglected, one can express the two particle correlation function in terms of the single particle source function, $\rho(r)$, and the two particle wave function $\Psi(r_1,r_2)$,

$$R(q)=\int d^3r_1 d^3r_2\ [|\Psi(r_1,r_2)|^2-1]\rho(r_1)\rho(r_2) \times[\int d^3r\rho(r)]^{-2}, \qquad (2)$$

Where $\rho(r) \propto \exp(-r^2/r^2_0)$.

Fig. 2 shows the two proton correlation function measured in this experiment. The curves are the theoretical calculations using eq.(2) for the values of the source radius r_0 indicated in the figure. Since finite emission times are neglected in the approximation taken in eq. (2), these values of r_0 only provide upper limits to the source size. Correlation functions for three energy gates are shown, each gate contains different proportion of equilibrium and non-equilibrium emission. Correlation functions for the low energy gate ($12MeV<E_1,E_2<25MeV$) are very similar suggesting that low energy protons may originate from the same reaction mechanism regardless of the angle of emission. The calculated curves show that low energy protons are consistent with a large or long lived source suggesting that these particles may be

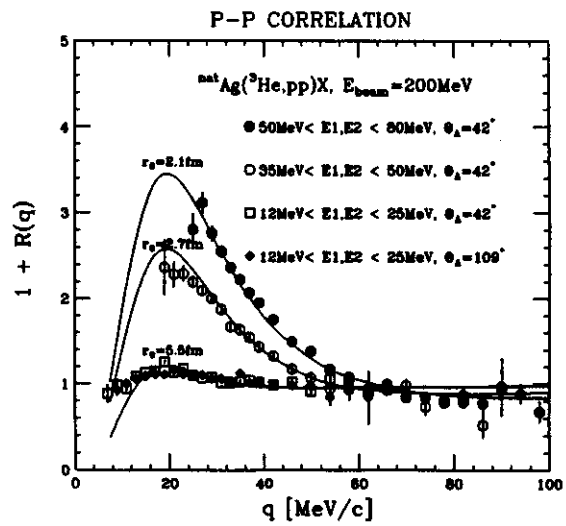

Fig. 2. P-P correlation functions measured in ^{3}He induced reactions on Ag at E_{beam} = 200 MeV. Three energy gates are put on the correlation function at the forward angles of θ_A = 42°. The correlation functions at the backward angles of θ_A = 109° is also shown for the low energy gate. The curves show calculated correlation functions for different value of r_0 using Eq. (2).

evaporated from a compound nucleus decay in the later stage of the reaction. For higher energy protons (35MeV<E_1,E_2<50MeV), the correlation functions are strongly enhanced at small relative momenta and for the highest energy gate (50MeV<E_1,E_2<80MeV) the correlation function is the largest we have measured. Such a large correlation function is consistent with a small source size suggesting the two protons are emitted from a more localized region during the early stages of the reaction.

---

a. Indiana University Cyclotron Facility, Bloomington, Indiana

References

1. S.E. Koonin, Phys. Lett. B 70(1977)43.
2. W.G. Lynch et. al., Phys. Rev. Lett. 51(1983)1850.
3. Z. Chen et. al., Phys. Rev. C 36(1987)2297.
4. D.A. Cebra et. al., Phys. Lett. B 227(1989)336.
5. T. Murakami et. al., Nucl. Instrum. Methods, A275(1989)112.

EMISSION TEMPERATURES FROM PARTICLE UNSTABLE COMPLEX NUCLEI

T.K. Nayak, T. Murakami, W.G. Lynch, K. Swartz[a], D.J. Fields[b], C.K. Gelbke, Y.D. Kim, J. Pochodzalla[c], M.B. Tsang, H.M. Xu, F. Zhu and K. Kwiatkowski[d]

Most of the models for fragmentation and emission of particle unstable complex nuclei in intermediate energy nuclear reactions use statistical concepts to explain the experimental observables such as the fragment mass distributions or the populations of ground and excited states of the fragments.[1,2] Statistical models frequently assume that the intrinsic degrees of freedom are fully thermalized and the asymptotic excited states of these fragments are populated statistically with weights determined by the excitation energy or temperature of the emitting system. Tests of this freezeout assumption can be made by comparing the measured relative populations of a large number of particle unstable states to the predictions of statistical calculations. In this article, we report the results of such a test.

Experimentally, the populations of particle unstable states were obtained by measuring the decay products in coincidence using a new high resolution position sensitive hodoscope.[3] Experimental population probabilities were extracted by fitting the spectra for the true coincidence yield to an appropriate R-matrix or Breit-Wigner formalism. Even with good energy resolution of the hodoscope (50 keV for 4.774 MeV state of ^{10}B), it was not possible to isolate each of the excited states in the experiment, and some neighboring states were grouped together statistically. In this fashion, population probabilities, defined with respect to the corresponding particle stable yields, were obtained for 40 groups of states in Li, Be, B, C, N and O isotopes.

Extensive calculations were performed to predict the population probabilities of these states while taking the sequential feeding effect from heavier particle unstable nuclei into account.[4] In these calculations, discrete and continuum states of nuclei with Z<13 were thermally populated and allowed to decay sequentially. Unknown spins, parities and isospins of lower lying discrete states were assigned according to primary distributions obtained from the non-interacting shell model. Calculations were repeated until their sensitivity to this unknown spectroscopic information could be assessed.

To provide a global test for statistical calculations, we have performed a least-squares analysis by computing

$$\chi^2_\nu = \frac{1}{\nu} \sum_{i=1}^{\nu} \frac{(y_{exp,i} - y_{cal,i})^2}{\sigma^2_\nu} \qquad (1)$$

for each initial temperature in the calculation. Here $y_{exp,i}$ and $y_{cal,i}$ are the experimental and calculated values of the population probability or ratios of population probabilities and ν is the number of data points. The uncertainty is given by $\sigma^2_i = \sigma^2_{exp,i} + \sigma^2_{cal,i}$ where $\sigma_{exp,i}$ is the experimental uncertainty, and $\sigma_{cal,i}$ reflects the range of calculated values. In the case of the ratios of population probabilities, all of the different quantities, $y_{exp,i}$ are not completely independent. This form of comparison was nevertheless chosen in order to provide a reasonable measure of the agreement between the measured and calculated quantities. Restricting the summation to only the mathematically independent quantities, such as the population probabilities would have made the χ^2_ν function unduly sensitive to the feeding corrections to

the populations of particle stable states.

Figure 1 shows the values of χ^2_ν computed from combinations of states, where the summation in Eq. 1 includes the data from the 40 groups of states which were measured for Li-O isotopes. The solid curve in the figure depicts the values of χ^2_ν where both the independent population probabilities and the ratios of population probabilities have been included. For comparison, we have included the dashed line in the figure which indicates the corresponding values for χ^2_ν when the sum in Eq. 1 is restricted to the independent population probabilities, and the dash-dotted line which shows the corresponding values when the sum is restricted to the ratios of population probabilities. The minimum value of χ^2_ν in these comparisons occurs for emission temperatures of T_{em}= 3-4 MeV. Also shown, as the dotted line in the figure is the χ^2_ν value for the single ratios involving the ^{5}Li ground state and 16.66 MeV excited state. Calculations indicate that

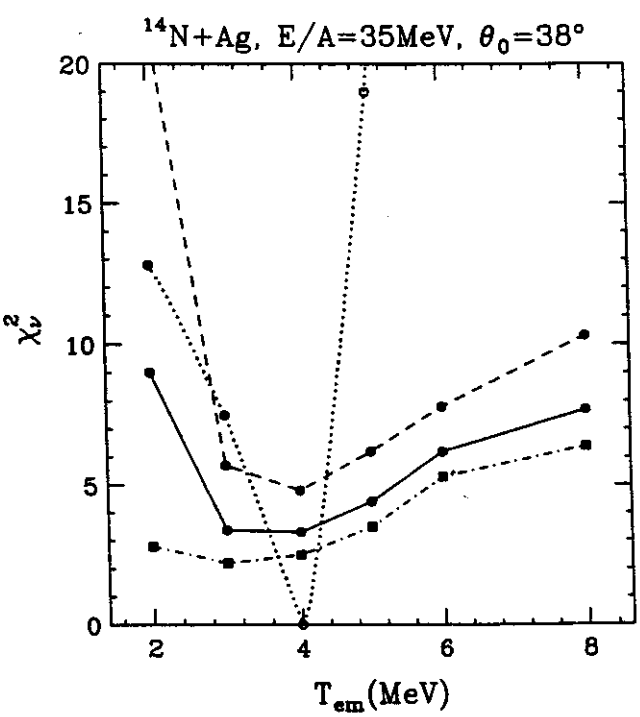

Fig. 1: Results of least-square analysis for a combination of all fragments. The lines are described in the text.

the relative populations of ^{5}Li excited states are rather insensitive to the sequential feeding from heavier particle unstable nuclei. For the ^{5}Li states, the minimum value of χ^2_ν occurs at T_{em}=4 MeV.

Even for T_{em}= 3-4 MeV, the values of χ^2_ν shown in Fig. 1 are rather large, indicating significant discrepancies between the measurements and calculations. This issue was investigated in greater detail for the case of excited ^{10}B states in ref (5). To explore this issue for other nuclei as well, we now present detailed comparisons between the experimental and calculated population probabilities and the ratios of population probabilities at T_{em} = 4 MeV. For these comparisons, we adopt the convention in which an apparent temperature T_{app} is defined by the relation:

$$\frac{n_i}{n_j} = \exp(-[E^*_i - E^*_j]\beta_{app}) \qquad (3)$$

where n_K and E_K, are the population probability and excitation energy of the Kth state of the unstable fragment and $\beta_{app} = 1/T_{app}$. (The population probability n_i corresponds to the average yield in an m-substate of the ith excited divided by the particle state yield.) If j denotes the ground state, we get

$$(2J_{g.s.}+1)n_i = \exp(-E^*_i \cdot \beta_{app}) \qquad (4)$$

where $J_{g.s.}$ is the spin of the ground state. The above equations define the apparent temperature T_{app} in terms of the measured or calculated values of n_i and n_j. Sometimes negative or infinite values for T_{app}, are obtained when these equations are applied to the experimental data. To avoid such singular behavior of the apparent temperature, we have extracted and assigned uncertainties to β_{app} rather than T_{app}.

In Figs. 2 and 3, we present values for β_{app} (on the lower axis) and T_{app} (on the upper axis) extracted from the population probabilities and ratios of population probabilities of states for isotopes with Z=5,6; Z=7; respectively. The solid points represent the values for β_{app} obtained from experimental population probabilities and the ratios of population probabilities. The histograms represent corresponding values for β_{ann} obtained from sequential feeding calculations starting with an initial temperature of T_{em} = 4 MeV. The uncertainties in the calculation are designated by the spread of the histogram which is shaded in the figure. In this figure, we have plotted only those cases where both the calculated or experimental uncertainties are smaller than the dynamic range of the figure.

The values for β_{app} and T_{app} obtained from measured and calculated population probabilities

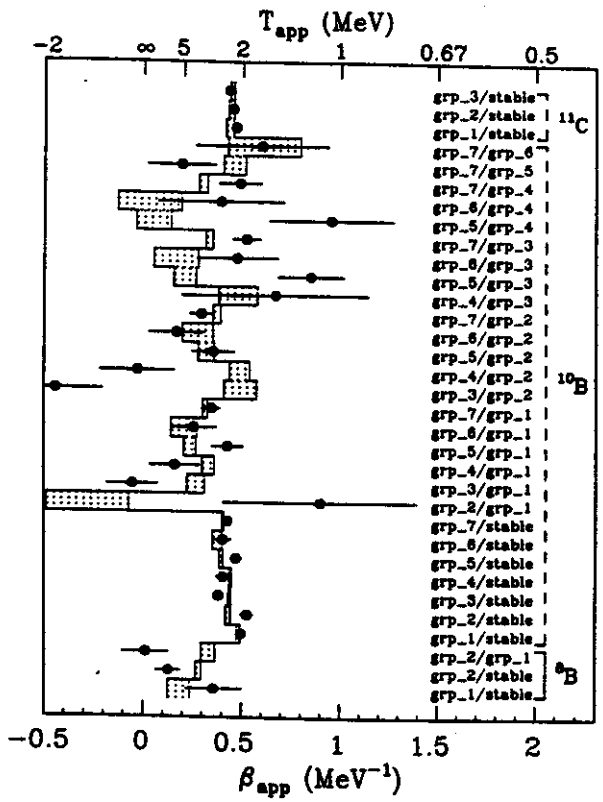

Fig. 2: Experimental values for β_{app} and T_{app} are shown as solid points for groups of excited states of B and C isotopes. The histograms represent the results of sequential feeding calculation with an initial temperature T_{em} = 4 MeV.

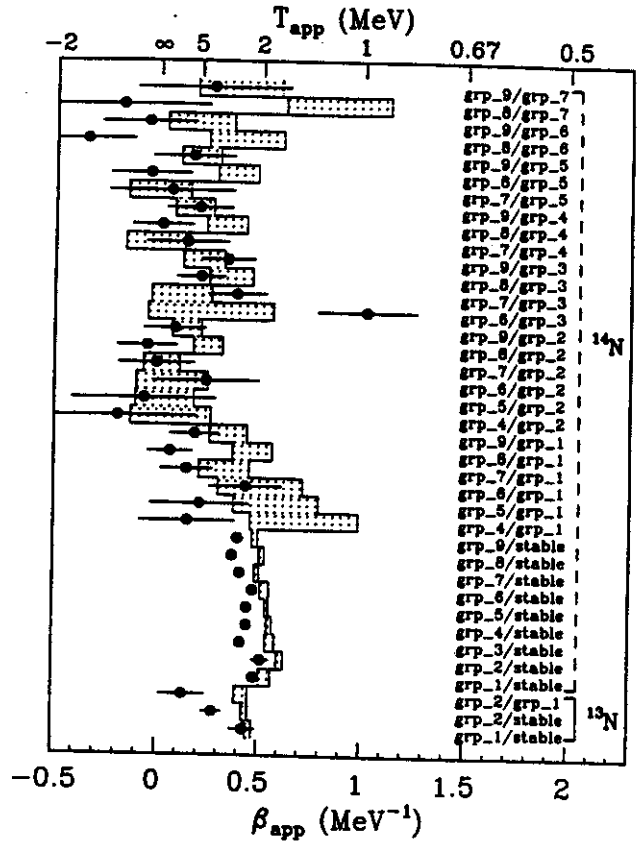

Fig. 3: Experimental values for β_{app} and T_{app} are shown as solid points for groups of excited states of ^{13}N and ^{14}N isotopes. The histograms represent the results of sequential feeding calculation with an initial temperature T_{em} = 4 MeV.

for two groups of states in ^{8}B, seven groups of states in ^{10}B and three groups of states in ^{11}C are presented in Fig. 2. For convenience of presentation, the ratios are labelled in the figure in terms of the groups of states. Details of these groupings of states, the fitting procedure, the spectroscopic information used in the fittings of these states, and the average population probabilities of each group of states will be given elsewhere.[6] Compared to the first excited state of ^{8}B (labeled as group 1), the measured population for the second excited state of ^{8}B (labeled as group 2) was larger than one would expect from the sequential feeding calculation. Even larger discrepancies are observed for the excited states of ^{10}B. Measured ratios involving the second group of

excited states at E*≈5.1 MeV and the third group of excited states at E*≈6 MeV are very strongly in disagreement with the calculations. In fact the ratio between the third and second groups gives a large negative apparent temperature in contrast to the predictions of the calculation. The groups of states for ^{11}C on the other hand, are well described by the calculations. Because of the large uncertainties in the calculated values for the ratios between excited states of ^{11}C, however, these ratios are not plotted.

In Fig. 3, we present β_{app} and T_{app} for two groups of states of ^{13}N and nine groups of states of ^{14}N. The experimental populations for the first group of ^{13}N are in agreement with the calculations. The deviation for the second group is large. The population probabilities in case of ^{14}N deviate significantly from the calculation for T_{em}=4 MeV, with, the calculation predicting somewhat more feeding to the particle stable states than observed. In this case, slightly better agreement is obtained with the population probabilities calculated for T_{em}=3 MeV. For the ratios of population probabilities, however, the agreement is actually better for T_{em}=4 MeV, and with the exception of the ratio of group 6 to group 3, the overall agreement is rather good.

In summary, it is an overall comparison of measured and calculated population probabilities of intermediate mass fragments emitted in ^{14}N induced reactions in Ag at E/A = 35 MeV indicate emission temperatures of about 3-4 MeV. A detailed comparison for individual fragments for a calculation with T_{em}= 4 MeV however, reveals that about half of all the experimental population probabilities and and one-third of the ratios of population probabilities showed significant deviations from the predictions of statistical calculations. The largest discrepancies in the ratios of excited state population probabilities were observed for ^{10}B, and in the population probabilities themselves, the largest discrepancies were observed for ^{14}N. Whether these discrepancies would be less in experiments with heavier or lighter beam where simple fragment production modes are suppressed is a question which should be addressed by future investigations.

---

a. Nuclear Physics Laboratory, University of Washington, Seattle, WA 98195.
b. Physics Division, Lawrence Livermore National Laboratory, Livermore, CA 94550.
c. Institut fur Kernphysik, Universitat Frankfurt, D-6000 Frankfurt, Federal Republic of Germany.
d. Department of Chemistry and Physics and Indiana university Cyclotron Facility, Indiana University, Bloomington, IN 47405.

References

1. W.G. Lynch, Ann. Rev. Nucl. Part. Sci. 37(1987)493.
2. "Proceedings of the Symposium on Central Collisions and Fragmentation Processes", edited by C.K. Gelbke, Nucl. Phys. A471C,(1987)1-451.
3. T. Murakami et. al. Nucl. Instrum. Method Phys. Res. Sect. A275(1989)112.
4. H.M. Xu et. al. Phys. Rev. C, 40(1989)186.
5. T.K. Nayak et. al. Phys. Rev. Lett., 62(1989)1021.
6. T.K. Nayak et. al., to be published.

THE ONSET OF SIMULTANEOUS MULTI-FRAGMENTATION

D.A. Cebra, S. Howden, J. Karn, A. Nadasen[a], E. Norbeck[b], C.A. Ogilvie[c], A. Vander Molen, G.D. Westfall, W.K. Wilson and J.S. Winfield

It has been proposed that a multi-fragment reaction mechanism should become dominant at excitation energies above 4 MeV/nucleon.[1-4] This process is related to the transition from the liquid to the gaseous phase of nuclear matter and should be characterized by a simultaneous dissociation of the system into many fragments. Identification of the threshold point for the onset of multi-fragmentation will provide information on the equation of state of nuclear matter. It has been demonstrated a definitive identification of this process requires study of an observable which is sensitive to the time scale of the disassembly.[5] Studies addressing this question of the fragmentation time scale have been attempted.[6-8] These studies span the excitation energy range from 1-6 MeV/nucleon, and all suggest that the disassembly occurs on slow time scale (a sequential process).

In this analysis we study the event shape,[4] which has been proposed to be an observable that is sensitive to the time scale of the fragmentation process.[5] The emission of fragments from a simultaneous multifragmentation process will be isotropic in the center-of-mass frame and therefore the events should be spherical in shape. Conversely, sequential emission should lead to an event shape that is elongated along one axis due to the kinematical constraints of the binary decays and the time ordered emission of the fragments. We shall compare the average event shapes extracted from our experimental data to predictions from simulations of both a sequential decay and a simultaneous multifragmentation.

We have studied the system $^{40}Ar+^{51}V$ using the MSU 4π Array[9] with beams provided by the K500 and K1200 cyclotrons. Six incident energies were studied: 35, 45, 55, 65, 75, and 85 MeV/nucleon. In the event shape analysis technique, one first transforms the observed event into the center-of-mass frame and then constructs a kinetic flow tensor

$$F_{ij} = \sum_n \frac{p_i^{(n)} p_j^{(n)}}{2m_n}$$

where $p_i^{(n)}$ denotes a momentum component of the n^{th} particle and m_n denotes its mass. One uses the ordered eigenvalues of this tensor, $t_1<t_2<t_3$, to define three reduced quantities

$$q_i = t_i^2 / \Sigma_{j=1}^{3} t_j^2$$

from which one determines the sphericity, $S=\frac{3}{2}(1-q_3)$, and the coplanarity, $C=\frac{1}{2}\sqrt{3}(q_2-q_1)$ as defined by Fai and Randrup[4] and applied to this problem by López and Randrup.[5]

We performed simulations of both sequential and simultaneous break-up processes. The sequential simulation assumed a stationary system with excitation energy from 8 to 20 MeV/nucleon which cooled through emission of energetic fragments. Events for the simultaneous simulation were generated from the events that had been produced by the sequential simulation. The emission directions were randomized, which corresponds to an isotropic emission. This technique ensured that the two simulations were identical with respect to the simple observables. These simulated events were filtered through software replica of our detector and analyzed in the same manner as our experimental data.

We first demonstrate that the inclusive

observables are correctly given by the simulations. Discrepancies in these observables will cause differences in the multi-particle observables that are unrelated to the effect of interest. Figure 1 displays these observables for the 65 MeV/nucleon case. The quantities that are compared include the both the total detected charged particle multiplicity and the multiplicity of identified particles, the mass and charge distributions, and the kinetic energy spectra for protons and Heliums. It is clear from Fig. 1 that the simulation accurately reproduces the basic observables of the experimental data. Similar reproductions of these observables have been obtained at the other energies studied.

Contour plots of the event shape distributions for the two simulations and for the experimental data are shown in Fig. 2 for the 65 MeV/nucleon case. Figure 2a displays the shape distribution for the sequential events. The distribution is sharply peaked around the

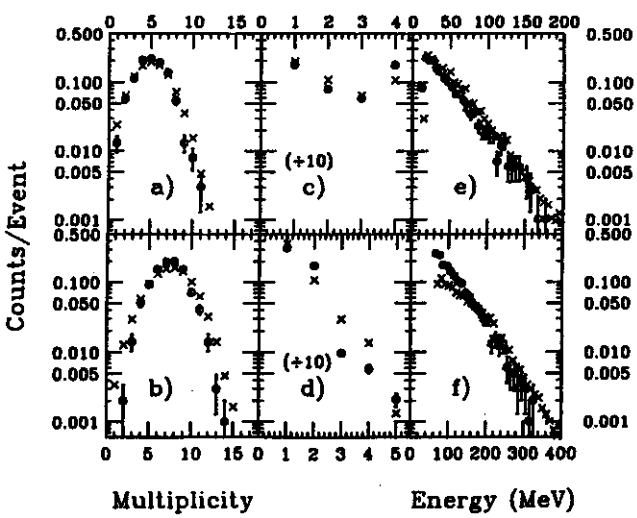

Fig. 1. A comparison of the results from simulations (O's) to the experimental (X's) data for the 65 MeV/nucleon case. Six observables are compared: a) the multiplicity of identified charged particles, b) total detected charged particle multiplicity (includes particles that stop in the ΔE scintillator), c) mass distributions for light particles, d) charge distributions, e) kinetic energy distributions for protons, and f) kinetic energy distributions for Heliums.

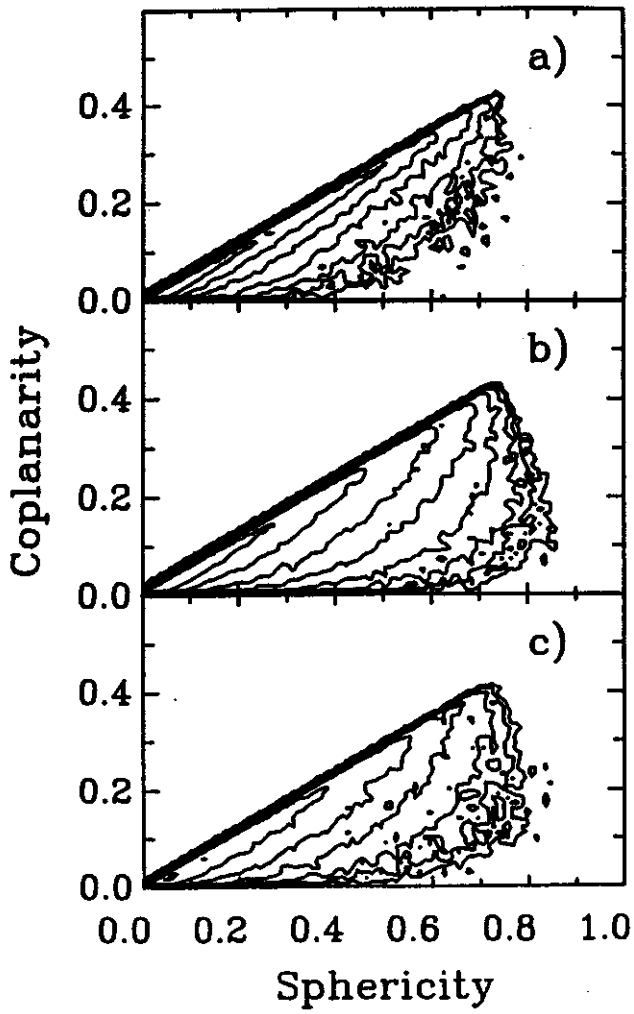

Fig. 2. Comparison of the distribution of event shapes for the 65 MeV/nucleon $^{40}Ar+^{51}V$ case from (a) a simulation of a sequential binary decay process, (b) the experimental data, and (c) a simulation of a simultaneous multi-fragmentation. Both simulations have been filtered through the acceptance of the MSU 4π Array. Three contours corresponds to one order of magnitude.

two dimensional axis, which suggests that the average event shape is that of a flattened prolate spheroid. The event shape distribution for the simultaneous simulation, which is displayed in Fig. 2c, is on average less prolate (a larger sphericity) than the sequential simulation. The shape distribution for the experimental data is shown in Fig. 2b. The events used for this analysis have been gated on impact parameter and only the most central ($\bar{b}$ =

0.3 b_{max}, where $b_{max} = R_{Ar} + R_V$) collisions have been selected. The determination of the centrality was made on an event by event basis using the total detected charge of fragments in the mid-rapidity range ($0.75y_{targ} < y_{frag} < 0.75y_{proj}$)[10].

The sphericity and coplanarity centroids of these two simulations and the experimental data are displayed on Fig. 3 for all the bombarding energies studied. The clear separation of the centroids from the two simulations confirms that this technique provides an observable capable of resolving between sequential and simultaneous multi-fragmentation. For the 35 MeV/nucleon case, the experimental centroids are almost identical to those predicted for sequential decay. For energies greater than 35 MeV/nucleon the experimental centroids fall between the two predicted values indicating that the pure sequential model does not apply for these energies. This suggests that a change in reaction mechanism has occured.

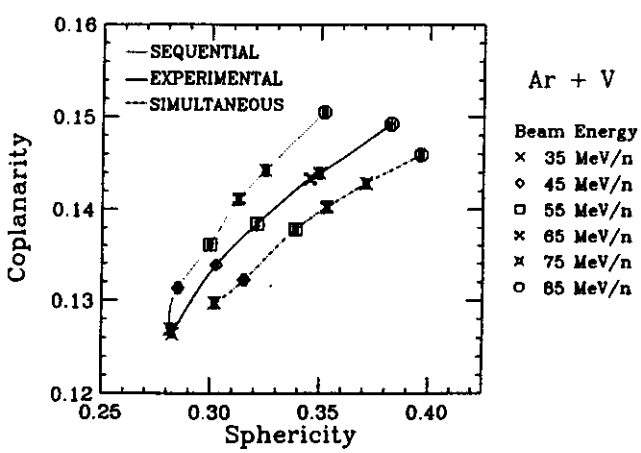

Fig. 3. A study of the average sphericity and coplanarity values as a function of beam energy for the system $^{40}Ar+^{51}V$. The centroids for the two simultaions and the experimental data are displayed for each beam energy. The lines (dotted for sequential, solid for experimental, and dotdash for simultaneous) are to guide the eye. The uncertainties displayed are statistical errors of the mean.

The data described in this work suggest that the onset of simultaneous multi-fragmentation may occur at excitation energies above 8 MeV/nucleon, which is the highest energy for which a sequential simulation can reproduce the multi-particle observables. The region from 8 to 20 MeV/nucleon may be a transition region where there is either a mixing of events representing the two precesses, a mixing of reaction processes during the course of an event, or a transitory process.

---

a. Permanent address University of Michigan, 4901 Evergreen Road, Dearborn MI 48128.
b. Permanent address Univeristy of Iowa, Iowa City, IA 52242.
c. Current address Gesellschaft fur Schwerionenforschung, D-6100 Darmstadt, West Germany.

References

1. J.P. Bondorf et al., Phys. Lett. B150(1985)57.
2. D.H.E. Gross et al., Phys. Rev. Lett. 56(1986)1544.
3. J. Randrup and S.E. Koonin, Nucl. Phys. A356(1981)223.
4. G. Fai and J. Randrup, Nucl. Phys. A404(1983)551.
5. J.A. López and J. Randrup, Nucl. Phys. A491(1989)477.
6. R. Bougault et al., Nucl. Phys. A488(1988)255c.
7. J. Pochodzalla, Nucl. Phys. A488(1988)353c.
8. J. Pouliot et al., Phys. Lett. B223(1989)16.
9. G.D. Westfall et al., Nucl. Inst. and Meth. A238(1985)347.
10. C.A. Ogilvie et al., Phys. Rev. C40(1989)654.